Interactions between growth-dependent changes in cell size, nutrient supply and cellular elemental stoichiometry of marine Synechococcus **(pre-proofs version of the manuscript)**

Nathan S. Garcia[a], Juan A. Bonachela[b] and Adam C. Martiny[a,c,1]

[a]Department of Earth System Science, 3200 Croul Hall, University of California, Irvine, California, USA, 92697

[b]Department of Mathematics and Statistics, Livingstone Tower, University of Strathclyde, 26 Richmond Street, Glasgow G1 1XH, Scotland, United Kingdom

[c]Department of Ecology and Evolution, 321 Steinhaus Hall, University of California, Irvine, California, USA, 92697

Running title: Cellular elemental stoichiometry of Synechococcus

Keywords: Redfield, chemostat, Cyanobacteria, physiology

[1]to whom correspondence should be addressed: ph: 949-824-9713 fax: 949-824-3874 amartiny@uci.edu

Abstract

The factors that control elemental ratios within phytoplankton like carbon:nitrogen:phosphorus (C:N:P), are key to biogeochemical cycles. Previous studies have identified relationships between nutrient-limited growth and elemental ratios in large eukaryotes, but little is known about these interactions in small marine phytoplankton like the globally important Cyanobacteria. To improve our understanding of these interactions in picophytoplankton, we asked how cellular elemental stoichiometry varies as a function of steady-state, N- and P-limited growth in laboratory chemostat cultures of Synechococcus WH8102. By combining empirical data and theoretical modeling, we identified a previously unrecognized factor (growth-dependent variability in cell size) that controls the relationship between nutrient-limited growth and cellular elemental stoichiometry. To predict the cellular elemental stoichiometry of phytoplankton, previous theoretical models rely on the traditional Droop model, which purports that the acquisition of a single limiting nutrient suffices to explain the relationship between a cellular nutrient quota and growth rate. Our study, however, indicates that growth-dependent changes in cell size play an important role. This key ingredient, along with nutrient-uptake-protein regulation, enables our model to predict the cellular elemental stoichiometry of Synechococcus across a range of nutrient-limited conditions. Our analysis also adds to the growth rate hypothesis, suggesting that P-rich biomolecules other than nucleic acids are important drivers of stoichiometric variability in Synechococcus. Lastly, our study indicates that abundant nutrients are not stored in high excess within Synechococcus. Our data provide a framework for understanding and predicting elemental ratios in ocean regions where small phytoplankton like Synechococcus dominates.

Introduction

A clear understanding of biogeochemical cycles is key to predicting long-term global change associated with rising atmospheric carbon dioxide (CO_2). The elemental composition of marine phytoplankton is central to ocean biogeochemistry as it links the global carbon (C) cycle with the cycling of other elements, such as nitrogen (N) and phosphorus (P) (Sterner and Elser, 2002; Galbraith and Martiny, 2015). The ratio of elements within organisms is known to vary with energy and nutrient flow through ecosystems (Sterner et al., 1997; Sterner and Elser, 2002; Urabe et al., 2002) and is linked to growth rates and nutritional status. The elemental stoichiometry of biological organisms propagates through the food web to shape community structure and function (Elser et al., 2000) and in turn, marine biota provides a flexible interface, linking global biogeochemical cycles together and can thereby have large effects on climate systems (Finkel et al., 2010; Galbraith and Martiny, 2015). Thus, factors that influence elemental stoichiometry of marine organisms are needed for refined models that forecast how the earth system will change in the future.

Models of biogeochemical cycles traditionally use a fixed ratio of C:N:P for major lineages of marine phytoplankton, even though C:N:P of phytoplankton can vary substantially. Countless studies indicate that cellular elemental stoichiometry is highly variable within isolates (Goldman et al., 1979; Geider et al., 1998; Geider and La Roche, 2002) and recent research indicates that C:N:P is also highly variable among ocean regions (Martiny et al., 2013; DeVries and Deutsch, 2014; Teng et al., 2014). Basic knowledge of the underlying physiological mechanisms that control this variability can provide a framework to understand and predict how marine biota interacts with biogeochemical cycles both now and in the future.

Cell models and the majority of laboratory studies have examined how multiple factors, such as growth rate and nutrient limitation interact to influence cellular elemental stoichiometry of phytoplankton. Basic physiological mechanisms link growth rates with chemical components within cells, which determine the cellular stoichiometry of elements. For example, the growth rate hypothesis (Sterner and Elser, 2002) predicts that ribosomes are needed in high concentrations when cells are growing fast, and the high P-content (~9%) in ribosomal RNA can cause changes in C:P and N:P with growth (Elser et al., 2000). Variability in other cell components, such as proteins (Rhee, 1978; Lourenço et al., 1998), pigments, phospholipids (Van Mooy et al., 2006) and polyphosphates (Rao et al., 2009; Martin et al., 2014), that are rich in a specific element like N or P, also contribute to variation in cellular elemental stoichiometry and may also co-vary with growth (Rhee 1973). Thus, variable nutrient supplies (e.g. N:P) are known to influence cellular biochemical content, which can affect growth and elemental stoichiometry of organisms (Rhee, 1978; Goldman et al., 1979; Geider and La Roche, 2002; Klausmeier et al., 2008).

Related to the growth rate hypothesis, empirical data have shown that C:P and N:P of phytoplankton varies when nutrients limit growth (Rhee, 1978; Goldman et al., 1979). This relationship has motivated the use of the classic Droop model to predict C:N:P as a function of growth in single- or multiple-nutrient theoretical models (Droop, 1968; Morel, 1987; Legović and Cruzado, 1997; Klausmeier et al., 2004a; Pahlow and Oschlies, 2009). In the Droop model, the growth rate of an organism increases hyperbolically as the cellular elemental quota of a single, growth-limiting nutrient (e.g. P) increases. Klausmeier et al. (2004a) used empirical data to build a Droop-based model in which growth rates decline due to decreasing concentrations of a limiting nutrient (e.g. NO_3^-), whereas other nutrients that are abundant (e.g. PO_4^{3-}) are acquired

to store a given element in excess. In other models, phytoplankton elemental stoichiometry results from resource allocation strategies and regulation of nutrient-uptake-proteins (Pahlow and Oschlies, 2009; Bonachela et al., 2013), which are known to comprise high portions (up to 50%) of cellular N in microbial organisms (Geider and La Roche, 2002). Thus, imbalanced nutrient supplies interact with growth rates to influence the cellular elemental composition through the ribosomal RNA, elemental storage, and nutrient acquisition mechanisms.

Nearly all of the systematic approaches to studying growth-dependent changes in cellular elemental stoichiometry have focused on large eukaryotic lineages, which are rare or absent from the large oligotrophic gyres throughout the world's oceans. While some studies have focused on small freshwater phytoplankton including Cyanobacteria (Healey, 1985; Claquin et al., 2002; Verspagen et al., 2014), less is known about these mechanistic relationships within marine Cyanobacteria, which are known to dominate vast nutrient-poor gyres (Flombaum et al., 2013). Recent estimates suggest that they contribute 25% of global marine net primary production and are found in most ocean regions in high abundance (Flombaum et al., 2013). Despite their large influence on global biogeochemical cycles, only a few studies have examined the cellular elemental stoichiometry of marine Cyanobacteria (Bertilsson et al., 2003; Heldal et al., 2003; Ho et al., 2003; Finkel et al., 2010) and even fewer have focused on physiological mechanisms that might control cellular C:N:P of lineages within Cyanobacteria (Fu et al., 2007; Kretz et al., 2015; Mouginot et al., 2015). Furthermore, none of these studies have examined the well-known interactive influence of growth physiology and nutrient supply on its cellular elemental stoichiometry. These relationships could be different in small phytoplankton in comparison with large phytoplankton, as cell size can reflect important differences in cellular physiology, such as the ability to store nutrients. Knowledge of basic mechanisms that regulate the C:N:P of

Cyanobacteria is essential to understand how this globally ubiquitous functional group of primary producers influences ocean biogeochemical cycles and how this influence might change in the future.

Here, we asked how cellular elemental stoichiometry of an isolate of one of the most numerically abundant phytoplankton genera in the global ocean (Flombaum et al., 2013), Synechococcus (WH8102), varies across a range of N- and P-limited steady-state growth rates in laboratory chemostat cultures. We also evaluated how nucleic acids contribute to cellular elemental stoichiometry by determining how cellular P is biochemically apportioned. Lastly, because we documented changes in cell size as a function of growth rate in our chemostat cultures, we used a theoretical model to ask how cell size contributes to relationships between nutrient-limited growth, elemental quotas and cellular elemental stoichiometry. Our results provide a basic understanding how one of the most abundant marine phytoplankton lineages regulates its elemental composition in the oceans.

Methods

Experiments

Using a modified method from Mouginot and co-workers (2015), cultures of Synechococcus (strain WH8102) were grown with a continuous dilution method in 8L-polycarbonate bottles at 24°C in an artificial seawater medium at ~195 μmol quanta m^{-2} s^{-1} on a 14:10 light:dark cycle. Light was supplied with cool white fluorescent lamps. We prepared artificial seawater modified from Waterbury and Willey (1988) (Supplementary Table S1), in 50L batches before autoclaving 7L volumes, to which, after cooling, we added 0.2-μm-filter-sterilized carbonates, trace metals, nitrate (NO_3^-) and phosphate (PO_4^{3-}) (Supplementary Table S1). Transfer of media and cultures to the chemostat system were done using a hood and open

137 flame to minimize contamination. The culturing system was enclosed with 0.2 μm-filtered air
138 pumped into the chamber with a 0.2 μm filter attached to an air outlet. We controlled the culture
139 dilution rate and hence the growth rate, by controlling the medium supply rate and the culture
140 volume. The liquid volume in the reservoirs ranged from 2.3 L to 5.25 L, thereby yielding a
141 range in dilution rates and steady-state growth rates with equivalent medium input rates. The
142 accumulation of cellular biomass was limited by NO_3^- (added as $NaNO_3$), where measured
143 nutrient concentrations in the medium were 15.9 μM NO_3^- and 9.2 μM PO_4^{3-} (added as K_2HPO_4)
144 yielding a $N:P_{input}$ supply ratio of 1.7, or by PO_4^{3-} with measured concentrations in the medium
145 of 38 μM NO_3^- and 0.56 μM PO_4^{3-}, yielding an $N:P_{input}$ supply ratio of 68. PO_4^{3-} and NO_3^- were
146 measured with a colorimetric assay as described in the Bermuda Atlantic Time-series Methods
147 (Michaels, Dow and Elardo, 1997; Michaels, Dow and Howse, 1997) with a spectrophotometer
148 (Genesis 10vis Thermo Scientific, Madison, WI, USA) at 885 and 543 nm, respectively.
149 Samples from chemostat cultures were collected on pre-combusted 450°C GF/F filters
150 (Whatman) for the analysis of particulate organic carbon (POC) and particulate organic nitrogen
151 (PON) (200 mL), particulate organic phosphorus (POP; 50 mL) and DNA and RNA (200 mL).
152 Samples for the analysis of POC and PON were dried at 50-80°C (48+ h), pelletized and
153 analyzed on a Flash EA 1112 NC Soil Analyzer (Thermo Scientific). Samples for the analysis of
154 POP were rinsed with 0.17 M $NaSO_4$, dried at 60-80°C with 2 mL of 0.017 M $MgSO_4$, and
155 combusted at 450°C for 2 h before adding 5 mL 0.2 M HCl and baking at 80-90°C. The resulting
156 orthophosphate concentrations were measured as described above.
157 Nucleic acids were measured by filtering cells onto combusted GF/F filters and storing
158 samples in liquid nitrogen until analysis. Cells were lysed with a bead-beater containing 1 mL of
159 a mixed solution containing 1 part RNA preservation solution (20 mM

ethylenediaminetetraacetic acid; 25 mM sodium citrate; and saturated with ammonium sulfate) and 4 parts 5 mM Tris buffer. Nucleic acids were measured in the supernatant with the Qubit dsDNA HS Assay Kit and the Qubit HS RNA Assay Kit (Invitrogen, Eugene, OR, USA) according to the method described by Zimmerman et al. (2014a; 2014b). This technique provides a linear signal in response to the amount of cell material analyzed and is able to recover nearly 100% of material from standards (from Qubit HS Assay Kit) that were spiked into the samples. Cells were counted with an Accuri C6 Flow Cytometer (Ann Arbor, MI, USA) by identifying particles with forward scatter (the proxy flow-cytometry estimate for cell size, FSCH) and Chl a fluorescence. Fluorescence of phycoerythrin was also determined with the flow cytometer. We estimated cell diameter with a cell-carbon/cell-volume conversion factor calculated with data acquired from a related Synechococcus strain (WH8103) growing in artificial seawater (Heldal et al., 2003). To summarize trends in steady-state responses to N and P-limited growth rates, we report the mean and standard deviations on measurements from samples collected on the final three time-points of the experimental trials. We fit the Droop model to the growth rate and elemental quota data in Figure 1 using a simple nonlinear least squares method with R statistical software (www.r-project.org) with the form $Q = a / (b - \mu)$, where $a = \mu_\infty \cdot Q'_{min}$, $b = \mu_\infty$, Q is elemental quota, and μ is growth rate.

Model

We used the empirical data from the chemostat cultures to expand on an existing model where cellular elemental stoichiometry emerges as a function of the nutrient-limited growth rate (See also Supplementary Information). This model uses physiological foundations similar to other models of cell stoichiometry (Lehman et al., 1975; Bonachela et al., 2013) and includes quota-regulated dynamics that encode changes in the number of nutrient-uptake proteins

(Bonachela et al., 2013). These dynamics depend on the quota of the nutrient that is taken up through the so-called expression function, F, and the P quota (as a proxy for the availability of protein-synthesizing ribosomes) through the repression function, G. The former encodes protein regulation strategies based on nutrient availability (upregulation for low nutrient, downregulation for high nutrient) (Dyhrman and Palenik, 2001). The latter, the feasibility of those strategies based on ribosome availability (e.g. low levels of RNA prevent synthesis from happening). For the number of proteins that take up N in the population, n_N, for example, these dynamics are given by the equation:

$$\frac{dn_N}{dt} = \nu_N H\left(1 - A_{rel}(t)\right) F\left(\frac{Q_{N_{max}} - Q_N(t)}{Q_{N_{max}} - Q_{N_{min}}}\right) G\left(\frac{Q_P(t) - Q_{P_{min}}}{Q_{P_{max}} - Q_{P_{min}}}\right) B(t) - w n_N(t), \quad (191)$$

where B represents population size, w is the dilution rate of the chemostat, ν_N is the maximum protein synthesis rate per cell and unit time, and H is a Heaviside function that depends on the ratio absorbing-to-total area (A_{rel}; i.e. a switch that stops protein synthesis when the absorbing area reaches the total area). As explained in the SI, n_N is positively correlated with the maximum uptake rate for nitrogen; in turn, n_P is positively correlated with the maximum uptake rate for phosphorus.

Unlike previous models, however, the maximum and minimum value for the quotas in our model (i.e. physiological ranges) are positively correlated with cell size (see SI, Eqs.(18)-(21)). These expressions are deduced from our laboratory data. Differently from previous models, we also de-couple the dynamics of population carbon and population number. While the dynamics of population carbon are somewhat controlled by the regulation of photosynthetic proteins [see SI Eq.(15)] and other metabolic expenses, the equation for the population number purely depends on cellular quota availability:

$$\frac{dB}{dt} = [f(Q_C, Q_N, Q_P) - w]B(t),$$

where f is a multiplicative function that depends on the three cellular elements. Thus, our expanded model implements variable cellular C quotas. Using different forms for the functional dependence between the C, N, and P quotas and the population dynamics of the chemostat cultures, f, allowed us to study how the emergent growth rates depend on the shape of this functional dependence (e.g. linear, Droop-like hyperbola).

All these components act as a feedback loop. From our chemostat cultures, we were able to deduce that the cellular growth rate influences the maximum C quota and that the cellular C quota influences the maximum and minimum N and P quotas. These extreme quotas are key to the regulation of the nutrient-uptake and photosynthetic proteins which, in turn, strongly influence nutrients and growth. As the cellular C quota is tightly correlated with cell size, the model ultimately links cell size and growth rate, which influence quota dynamics and elemental stoichiometry. See SI for further details.

Results

To understand the interaction between nutrient-limitation, growth physiology, and cellular elemental stoichiometry, we analyzed steady-state chemostat cultures of Synechococcus WH8102 across four growth rates and two different nutrient supply regimes ($N:P_{input}$ = 1.7 and $N:P_{input}$ = 68). First, we monitored the culture cell density, cell size and particulate organic matter in cultures to ensure they were growing at steady-state (Supplementary Figure S1). Both residual dissolved PO_4^{3-} in P-limited cultures and residual dissolved NO_3^- in N-limited cultures were below the detection limit of the spectrophotometric methods used. This indicated that the biomass in cultures, and hence the physiology of cells, were strongly P- or N-limited, respectively (Supplementary Figure S2). In addition, the sum of the residual dissolved PO_4^{3-} and

228 NO_3^- with POP and PON concentrations, respectively, were close to measured input
229 concentrations of PO_4^{3-} and NO_3^-. This indicated that cells were able to drawdown nearly all of
230 the PO_4^{3-} or NO_3^- supplied to P- or N-limited chemostat cultures, respectively (Supplementary
231 Figure S2). Hence, estimates of culture cell densities, cellular elemental stoichiometry ($C:P_{cell}$
232 and $N:P_{cell}$) and residual nutrient concentrations suggested that cells had reached a steady-state
233 by the end of each chemostat trial (Supplementary Figure S1-S3).

234 Growth rate and culture cell density varied in a negative relationship, with a stronger
235 relationship in P-limited vs. N-limited cultures (Supplementary Figure S1A-C). In contrast, the
236 proxy flow-cytometry estimate for cell size (FSCH) was positively related to growth rate in
237 steady-state chemostats under both N- and P-limitation (Supplementary Figure S1D-F).
238 Throughout each trial, POC decreased as a function of P-limited growth rate but was relatively
239 invariable under N-limited growth (Supplementary Figure S1G-I).

240 The steady-state cellular elemental quotas of C, N, and P (Q_C, Q_N, and Q_P) all increased
241 as a function of growth following a hyperbolic curve resembling the Droop model equation ($r^2 \geq$
242 0.94, Figure 1 and Table 1). To quantify physiological limits on growth rates and elemental
243 quotas, we defined μ_∞ and Q'_{min} as the conditional maximum growth rate and the conditional
244 minimum elemental quota, respectively, given the ambient light and temperature levels in our
245 experiments. Although the conditional minimum C and N quotas ($Q'_{C,min}$, $Q'_{N,min}$) did not vary
246 between P-limited and N-limited cells (student's t-test, $P > 0.05$, Figure 1a, Table 1), the
247 conditional minimum P quota ($Q'_{P,min}$), significantly increased by 118-146% under N-limited
248 conditions in comparison with P-limited conditions (Figure 1c, Table 1). Also, in P-limited
249 cultures, μ_∞ was significantly higher (student's t-test, $P < 0.05$) when calculated from the Q_C or
250 Q_N data in comparison with that calculated from the Q_P data (Table 1). Collectively, these

differences reflect strong differences in the cell quotas as a function of growth and nutrient conditions (Figure 1a-c).

The observed increase in cell quotas with growth rate could lead to changes in overall cell size (Figure 2a). To further examine this, we compared a flow-cytometric metric for cell size (FSCH) with growth rates. Growth physiology had a significant effect on FSCH (analysis of covariance test, $F_{1,32} = 239$, $P < 0.001$; Figure 2b). In addition, growth rate and limitation type (N or P) had a significant interactive effect on FSCH (analysis of covariance test, $F_{1,32} = 13$, $P = 0.001$). This interactive effect indicated that N-limited cells were larger than P-limited cells when the growth rate was high (analysis of covariance test, $F_{1,32} = 122$, $P < 0.001$), but the effect of limitation type on FSCH was reduced in slower-growing cells (Figure 2b). We also compared FSCH with other cellular measurements. Cellular nucleic acids (DNA_{cell} and RNA_{cell}, Supplementary Figure S5A and B), pigment fluorescence (fluorescence of Chl a and phycoerythrin; Supplementary Figure S4C and D), and cell quotas (Supplementary Figure S4) all varied in a positive linear relationship with FSCH (t-test, $P < 0.05$) regardless of limitation type (Supplementary Figure S1). Thus, the effect of growth on cell size was linked to a general increase in cellular mass. Furthermore, the fluorescence of cellular pigments (Chl. a and phycoerythrin) was elevated under P-limitation in comparison with N-limitation (analysis of covariance, $F_{1,32} > 9$; $P < 0.05$; Supplementary Figure S4C and D), suggesting an additional effect of limitation type.

We next identified the role of nucleic acids in setting Q_P, as P in RNA has previously been shown to be an important driver of elemental stoichiometry (Sterner and Elser, 2002). First, we observed that the proportion of Q_N in nucleic acids increased as a function of growth under both N- and P-limitation, reflecting the general positive relationship between growth and cellular

nucleic acid concentrations (Figure 3a, triangles). Despite this positive relationship, the proportion of Q_P devoted to nucleic acids (Figure 3b and c) declined as a function of increasing growth in P-limited cultures ($P < 0.05$; Figure 3a, closed circles). This declining contribution suggested that P-containing cellular resources other than nucleic acids also varied in a positive relationship with P-limited growth. This effect was not observed under N-limitation, however, suggesting a tradeoff between non-nucleic acid, P-containing cellular resources or function under N-limited growth (e.g. between storage and physiologically active P-containing resources; Figure 3a).

We then identified trends in cellular elemental stoichiometry of Synechococcus. $C:P_{cell}$ and $N:P_{cell}$ of Synechococcus declined as a linear function with increasing growth (t-test, $P < 0.05$; Figure 4a and b) under P limitation. In contrast to the negative linear relationship between $N:P_{cell}$ and P-limited growth, $N:P_{cell}$ was stable under N-limited growth (t-test, $P > 0.05$). $C:P_{cell}$ only decreased marginally with N-limited growth (t-test, $P < 0.05$, Figure 4b). $C:N_{cell}$ was generally elevated in slow-growing N-limited cultures in comparison with slow-growing P-limited cultures, but was more variable at higher growth rates (Figure 4c). Because of the strong contrast between our observations, some previous findings, and models of phytoplankton stoichiometry under N-limitation, we repeated our N-limited trials with Synechococcus and ensured our results could be replicated (Figure 4).

While the observed behavior of Q_P and Q_N initially mimicked Droop model curves, we were not able to replicate empirical trends in cellular elemental ratios by using existing Droop-based variable quota models nor by using more mechanistic quota-based models with fixed minimum and maximum elemental quota values (Klausmeier et al., 2004a; Legović and Cruzado, 1997). We tested whether the absence of a link between growth-dependent changes in

297 all three elemental quotas and cell size (common to all existing models) is the reason for this
298 failure to replicate our data. Thus, we modified an existing physiological model (Bonachela et
299 al., 2013) to include growth-dependent changes in cell size that influence cellular elemental
300 quotas as well as their maximum and minimum values, which in turn are key in the regulation of
301 nutrient-uptake proteins (see Supplementary Information). Our expanded model captures the
302 observed relationship between cellular elemental stoichiometry and growth (Figure 4) including
303 the "Droop-like" behavior for all cellular elemental quotas. Only the inclusion of growth-
304 dependent cell size and quota-dependent protein regulation enabled the replication of the
305 observed behavior. Importantly, these two key underlying mechanisms are fundamentally
306 different than those in the Droop model, and confirm the strong influence of cell size on the
307 resulting cellular elemental quotas and ratios.

308 **Discussion**

309 Using controlled chemostat cultures of an isolate representing one of the most abundant
310 marine phytoplankton lineages, we observed strong inconsistencies between our data and some
311 fundamental conceptual mechanisms that have commonly been invoked to understand the
312 elemental composition of phytoplankton. First, although RNA_{cell} and DNA_{cell} increased with
313 increasing growth rate, thereby supporting a key aspect of the growth rate hypothesis (Sterner
314 and Elser, 2002). However, the proportion of Q_P devoted to nucleic acids did not increase with
315 increasing growth, suggesting that P in nucleic acids is not the central driver of the cellular
316 elemental stoichiometry of Synechococcus within this growth rate range. Our estimates of this
317 proportion agree with previous estimates indicating that RNA_{cell} is low in Synechococcus
318 (Mouginot et al., 2015) and imply that P-rich biomolecules other than nucleic acids also co-vary
319 with growth (Figure 3). Nucleic acids might have a more dominant influence when growth rates

320 are very close to μ_{max}, however, and in absence of μ_{max} data for WH8102, our high growth rate
321 cultures represent ~67-73% of μ_{max} of a related isolate of Synechococcus (Moore et al., 1995).
322 Nucleic acids might also have a stronger influence on stoichiometric differences across lineages
323 where maximum growth rates are vastly different (Elser et al., 2000), rather than within a single
324 isolate.

325 A second departure from the accepted conceptual models of cellular elemental
326 stoichiometry is the observed role of cell size and associated quotas as a function of growth.
327 Although none of the previous theoretical models include growth-dependent variability in cell
328 size, our data indicate that cell size and all of the cell components that we measured (Q_C, Q_N, Q_P,
329 DNA_{cell}, RNA_{cell}, and cellular pigment fluorescence) were positively related to the cellular growth
330 rate (Figure 2, Supplementary Figures S4 and S5). Thus, cell size is a critical ingredient in our
331 expanded model of cellular elemental stoichiometry because it allows Q_C, Q_N, and Q_P to change
332 as a function of growth, however disproportionately. In support of this, some previous data
333 acknowledge growth-dependent changes in cell size of phytoplankton (Cook, 1963). However,
334 Q_C or cell size has typically been held constant under variable growth rates in previous
335 theoretical models (e.g., Shuter, 1979; Klausmeier et al., 2008; Bonachela et al., 2013). Instead,
336 theoretical models typically rely on the Droop model equation to describe growth-dependent
337 relationships in the ratios of cellular elements. The positive relationship between cell size and
338 growth rate is a common observation within specific isolates of microbes and has been termed
339 the growth rate law (Schaechter et al., 1958; Vadia and Levin, 2015).

340 Although the Droop model equation fits our Q_N and Q_P data well, the model's underlying
341 mechanism is fundamentally different than the cell-size/growth-rate relationship. The traditional
342 Droop model focuses on growth-dependent changes in a single growth-limiting elemental quota

343 (such as Q_N or Q_P), whereas our data demonstrate that the cell-size/growth relationship
344 contributes to growth-dependent changes in all three of the cellular elemental quotas that we
345 measured. For example, the Droop model fits our Q_C data very well, but this fit did not result
346 from carbon limitation, as the Droop model would predict. Instead, changes in Q_C were directly
347 related to growth-dependent changes in cell size, and the Droop model coincidentally fit these
348 changes in cell size, which did not result from differences in the carbon supply. This is also
349 evident from our Q_N data, which follow the Droop model relationship in contrasting P-limited
350 chemostats. Under P-limited growth, nitrate was in high abundance but Q_N fit the Droop model
351 in nearly the same way as N-limited cells (Fig. 1b). Therefore, the Droop model fit to Q_N and Q_P
352 do not result directly from N or P acquisition, but instead, as our model confirms, results from
353 the cell-size/growth-rate relationship. Thus, by decoupling the equations for the population
354 carbon and number of cells, we achieved a dynamic regulation of Q_C (and hence a cell-
355 size/growth-rate link), which together with the dynamics of Q_N and Q_P and their effect on protein
356 regulation, was necessary to predict our observed trends in cellular elemental stoichiometry of
357 Synechococcus.

358 In contrast with Droop-based models of phytoplankton stoichiometry, where $C:P_{cell}$ and
359 $N:P_{cell}$ change sharply as a function of P-limited growth (Klausmeier et al., 2004a; Bonachela et
360 al., 2013), our model and data indicate that $C:P_{cell}$ and $N:P_{cell}$ of Synechococcus decrease almost
361 linearly as a function of P-limited growth (Figure 4a and b). We also obtained marginal changes
362 in $C:P_{cell}$ and no change in $N:P_{cell}$ as a function of N-limited growth, and collectively, these
363 trends have been observed in other phytoplankton (Goldman et al., 1979). The invariable $N:P_{cell}$
364 under N-limited growth is remarkable for the globally abundant Synechococcus because $N:P_{cell}$ is
365 consistently close to the Redfield ratio (16) even under severe N-limitation, a common state

among field populations (Moore et al., 2013). Understanding environmental controls on cellular elemental stoichiometry in the small but dominant prokaryotic phytoplankton lineages under N-limitation might be key to understanding the primary drivers of Redfield stoichiometry in the oceans. But the mechanisms that contribute to variability in cellular elemental stoichiometry may be different for different lineages because this invariable trend does not appear to be consistent across lineages of phytoplankton (Goldman et al., 1979).

We also observed moderate decreases in $C:N_{cell}$ under severely P-limited growth in comparison with severely N-limited growth, which seem to be related to cell size and pigment fluorescence (Fig. 4). N-limited cells were larger than P-limited cells, evident from differences in FSCH (Figure 2) and Q_C (Figure 1a) between these two treatments. Despite differences in cell size, Q_N was relatively invariable between N and P-limited cells (Figure 1b). This generally resulted in elevated $C:N_{cell}$ in slow-growing N-limited cells in comparison with other treatments (Figure 4c), which, based on our pigment fluorescence data, seems to be caused by higher cellular concentrations of N-rich pigments in P-limited cells (Supplementary Figure S5C and D). Since phycoerythrin, a dominant pigment in Synechococcus (Scanlan et al., 2009), is composed of protein, and proteins comprise a large portion of Q_N (Rhee, 1978; Lourenço et al., 1998), the rigidity in Q_N between P- and N-limited cells may be caused by differences in phycoerythrin, which is known to play a dual role in photosynthesis and N-storage (Wyman et al., 1985; Yeh et al., 1986). Thus, the decline in $C:N_{cell}$ in severely P-limited cells seems to result from the combined effect of smaller cells and higher pigment fluorescence in comparison with severely N-limited cells.

In general, small phytoplankton are thought to lack major nutrient storage reservoirs. Aside from differences in cellular pigment fluorescence, we did not observe signs of abundant N

389 or P storage in Synechococcus. Some theoretical models rely on cellular storage components to
390 predict cellular stoichiometry (Daines et al., 2014), but our observed changes in Q_N with growth
391 were mainly dependent on changes in cell size, regardless of limitation type. This observation is
392 consistent with the general lack of the major N-storage compound – cyanophycin - in
393 Synechococcus isolates (Wingard et al., 2002). In models, Q_N or Q_P increase as a function of
394 decreasing growth in environments, where N or P is abundant, respectively (i.e. where P or N is
395 limiting growth, respectively) (Klausmeier et al., 2004a; Klausmeier et al., 2008). Although
396 pigments probably contributed to minor N storage under slow P-limited growth, the large
397 increases in $N:P_{cell}$ (Figure 4b) in our experiments did not result from abundant increases in
398 cellular N storage, as Q_N was roughly linked to cell volume (Supplementary Figure S6A, closed
399 symbols). Instead, the strong variation in $N:P_{cell}$ as a function of P-limited growth (Figure 4b)
400 resulted from stronger changes in Q_P (Figure 1c) relative to moderate changes in cell size (i.e.
401 Q_C) (Figure 1a) and relative to small changes in Q_N under N-limitation. Even under slow N-
402 limited growth, cells did not store P in high excess either; changes in Q_P in P-replete
403 environments were also tightly linked to changes in cell volume (Supplementary Figure S6B,
404 open symbols). Thus, the major variation in $C:P_{cell}$ and $N:P_{cell}$ within Synechococcus (Figure 4a
405 and b) seems to be driven by a larger change in Q_P relative to changes in cell size (Q_C) and Q_N
406 under P-limited growth, in comparison with small changes in Q_N relative to changes in cell size
407 (Q_C) and Q_P under N-limited growth. But we did not observe drastic increase in Q_P or Q_N under
408 different N- or P-limited environments as modeled previously (Klausmeier et al., 2004a),
409 indicating that N and P were not stored in high abundance in N- or P-replete environments,
410 respectively.

411 In consideration of how C:P_{cell} and N:P_{cell} varies relative to cell size (Q_C) and Q_N in P-
412 and N-limited environments, we postulate that variable cell concentrations of P-rich
413 biomolecules must be major drivers of stoichiometric variation in Synechococcus. Cellular
414 phospholipid concentrations are known to decline under P-limitation (Van Mooy et al., 2006) but
415 in general do not represent a large proportion of cellular P (Mouginot et al., 2015). Although
416 much less is known about polyphosphates in Cyanobacteria, they may also co-vary with growth
417 in Synechococcus, as documented in another species of phytoplankton (Rhee, 1973). While some
418 data suggest that the adenylate pool increased with increasing growth rate in heterotrophic
419 Bacteria (Marriot et al., 1981), adenosine triphosphate in Synechococcus WH8102 was highly
420 correlated with FSCH regardless of the chemostat dilution rate and represented less than 1% of
421 Q_P in another experiment (unpublished data). The general lack of major storage reservoirs in
422 small Cyanobacteria may be key to distinguishing trends in cellular elemental stoichiometry
423 from those in larger phytoplankton, as previous data with diatoms suggest that Q_C increases with
424 decreasing P-limited growth (Laws and Bannister, 1980), contrasting the diminishing Q_C with
425 decreasing growth of Synechococcus (Figure 1a).

426 Ecological implications

427 Our results may be applied to broadly understand the physiological status of unicellular
428 Cyanobacteria in the ocean. If we compare our results with stoichiometric data compiled by
429 Martiny et al. (2013) and inversely estimated by Teng et al. (2014), the high C:P ratios observed
430 in the P-limited North Atlantic Subtropical Gyre (Lomas et al., 2010; Moore et al., 2009) are
431 congruent with C:P_{cell} of Synechococcus when growth rates are strongly P-limited. In contrast,
432 the moderate C:P ratios (but above Redfield proportions) observed in the presumed N-limited
433 Southern Atlantic Subtropical Gyre (Teng et al., 2014) are similar to the C:P ratios that we

observed in slower growing N-limited cultures. The low C:P estimates in the eastern equatorial Atlantic upwelling region (where nutrients are abundant) are consistent with a high frequency of fast-growing Synechococcus cells. Thus, our data and model seem to corroborate the physiological status of biota in major ocean basins and our observations suggest that cell size and lack of elemental storage capacity influence cellular elemental stoichiometry of small marine phytoplankton within field populations. In comparison with data collected from other species of phytoplankton, our findings further suggest that fundamentally different biochemical mechanisms might control the cellular elemental stoichiometry of small vs. large phytoplankton, such as Cyanobacteria vs. eukaryotes. Such biochemical mechanisms can contribute to understanding broad scale patterns in ocean biogeochemistry and regional differences in C:N:P. As studies of environmental controls on cellular elemental stoichiometry emerge among broader lineages of phytoplankton, we might begin to forecast how ocean biogeochemical cycles will respond to global change.

Acknowledgments

Support for this research was provided by the UCI Chancellor's ADVANCE Postdoctoral Program and the National Science Foundation Dimensions of Biodiversity (OCE-1046297) and Major Research Instrumentation programs (OCE-1126749). JAB acknowledges support of the MASTS pooling initiative (The Marine Alliance for Science and Technology for Scotland). MASTS is funded by the Scottish Funding Council (grant reference HR09011) and contributing institutions.

Conflict of Interest

The authors declare no conflict of interest.

457 Supplementary Information accompanies this paper on The ISME Journal website.

458 **References**

459 Bertilsson S, Berglund O, Karl DM, Chisholm SW. (2003). Elemental composition of marine
460 Prochlorococcus and Synechococcus: Implications for the ecological stoichiometry of the sea.
461 Limnol Oceanogr **48**: 1721–1731.

462 Bonachela JA, Allison SD, Martiny AC, Levin SA. (2013). A model for variable phytoplankton
463 stoichiometry based on cell protein regulation. Biogeosciences **10**: 4341–4356.

464 Claquin P, Martin-jézéquel V, Kromkamp JC, Veldhuis MJW, Kraay GW. (2002). Uncoupling
465 of silicon compared with carbon and nitrogen metabolisms and the rol of the cell cycle in
466 continuous cultures of Thalassiosira pseudonana (Bacillariophyceae) under light, nitrogen, and
467 phosphorus control. J Phycol **38**: 922–930.

468 Cook JR. (1963). Adaptations in growth and division in euglena effected by energy supply. J
469 Protozool **10**: 436–444.

470 Daines SJ, Clark JR, Lenton TM. (2014). Multiple environmental controls on phytoplankton
471 growth strategies determine adaptive responses of the N : P ratio. Ecol Lett **17**: 414–425.

472 DeVries T, Deutsch C. (2014). Large-scale variations in the stoichiometry of marine organic
473 matter respiration. Nat Geosci **7**: 890–894.

474 Droop MR. (1968). Vitamin B_{12} and marine ecology. IV. The kinetics of uptake, growth and
475 inhibtition in Monochrysis lutheri. J Mar Biol Ass UK **48**: 689–733.

476 Dyhrman ST, Palenik B. (2001). A single-cell immunoassay for phosphate stress in the
477 dinoflagellate Prorocentrum minimum (Dinophyceae). J Phycol **37**: 400–410.

478 Elser JJ, O'Brien WJ, Dobberfuhl DR, Dowling TE. (2000). The evolution of ecosystem
479 processes: growth rate and elemental stoichiometry of a key herbivore in temperate and arctic
480 habitats. J Evol Biol **13**: 845–853.

481 Elser JJ, Sterner RW, Gorokhova E, Fagan WF, Markow TA, Cotner JB, et al. (2000). Biological
482 stoichiometry from genes to ecosystems. Ecol Lett **3**: 540–550.

483 Finkel Z V, Beardall J, Flynn KJ, Quigg A, Rees TA V, Raven JA. (2010). Phytoplankton in a
484 changing world: cell size and elemental stoichiometry. J Plankton Res **32**: 119–137.

485 Flombaum P, Gallegos JL, Gordillo RA, Rincón J, Zabala LL, Jiao N, et al. (2013). Present and
486 future global distributions of the marine Cyanobacteria Prochlorococcus and Synechococcus.
487 Proc Natl Acad Sci U S A **110**: 9824–9.

488 Fu FX, Warner ME, Zhang Y, Feng Y, Hutchins DA. (2007). Effects of increased temperature
489 and CO_2 on photosynthesis, growth, and elemental ratios in marine Synechococcus and
490 Prochlorococcus (Cyanobacteria). J Phycol **43**: 485–496.

491 Galbraith ED, Martiny AC. (2015). A simple nutrient-dependence mechanism for predicting the
492 stoichiometry of marine ecosystems. Proc Natl Acad Sci **112**: 201423917.

493 Geider R, La Roche J. (2002). Redfield revisited: variability of C:N:P in marine microalgae and
494 its biochemical basis. Eur J Phycol **37**: 1–17.

495 Geider RJ, MacIntyre HL, Kana TM. (1998). A dynamic regulatory model of phytoplanktonic
496 acclimation to light, nutrients, and temperature. Limnol Oceanogr **43**: 679–694.

497 Goldman JC, McCarthy JJ, Peavey DG. (1979). Growth rate influence on the chemical

composition of phytoplankton in oceanic waters. Nature **279**: 210–215.

Healey F. (1985). Interacting effects of light and nutrient limitation on the growth rate of Synechococcus linearis (Cyanophyceae). J Phycol **21**: 134–146.

Heldal M, Scanlan DJ, Norland S, Thingstad F, Mann NH. (2003). Elemental composition of single cells of various strains of marine Prochlorococcus and Synechococcus using X-ray microanalysis. Limnol Oceanogr **48**: 1732–1743.

Ho T-Y, Quigg A, Finkel ZV, Milligan AJ, Wyman K, Falkowski PG, et al. (2003). The elemental composition of some marine phytoplankton. J Phycol **39**: 1145–1159.

Klausmeier CA, Litchman E, Daufresne T, Levin SA. (2004). Optimal nitrogen-to-phosphorus stoichiometry of phytoplankton. Nature **429**: 171–174.

Klausmeier CA, Litchman E, Daufresne T, Levin SA. (2008). Phytoplankton stoichiometry. Ecol Res **23**: 479–485.

Klausmeier CA, Litchman E, Levin SA. (2004). Phytoplankton growth and stoichiometry under multiple nutrient limitation. Limnol Oceanogr **49**: 1463–1470.

Kretz CB, Bell DW, Lomas DA, Lomas MW, Martiny AC. (2015). Influence of growth rate on the physiological response of marine Synechococcus to phosphate limitation. Front Microbiol **6**: 6–11.

Laws EA, Bannister TT. (1980). Nutrient- and light-limited growth of Thalassiosira fluviatilis in continuous culture, with implications for phytoplankton growth in the ocean. Limnol Oceanogr **25**: 457–473.

Legović T, Cruzado A. (1997). A model of phytoplankton growth on multiple nutrients based on the Michaelis-Menten-Monod uptake, Droop's growth and Liebig's law. Ecol Modell **99**: 19–31.

Lehman JT, Botkin DB, Likens GE. (1975). The assumptions and rationales of a computer model of phytoplankton dynamics. Limnol Oceanogr **20**: 343–364.

Lomas MW, Burke AL, Lomas DA, Bell DW, Shen C, Dyhrman ST, et al. (2010). Sargasso Sea phosphorus biogeochemistry: an important role for dissolved organic phosphorus (DOP). Biogeosciences **7**: 695–710.

Lourenço SO, Barbarino E, Marquez UML, Aidar E. (1998). Distribution of intracellular nitrogen in marine microalgae: Basis for the calculation of specific nitrogen-to-protein conversion factors. J Phycol **34**: 798–811.

Marriot ID, Edwin AD, Rowley BI. (1981). Effect of growth rate and nutrient limitation on the adenine nucleotide content , energy charge and enzymes of adenylate metabolism in Azotobacter beijerinckii. J Gen Microbiol **125**: 375–382.

Martin P, Dyhrman ST, Lomas MW, Poulton NJ, Van Mooy BAS. (2014). Accumulation and enhanced cycling of polyphosphate by Sargasso Sea plankton in response to low phosphorus. Proc Natl Acad Sci U S A **111**: 8089–94.

Martiny AC, Pham CTA, Primeau FW, Vrugt JA, Moore JK, Levin SA, et al. (2013). Strong latitudinal patterns in the elemental ratios of marine plankton and organic matter. Nat Geosci **6**: 279–283.

Michaels A, Dow R, Elardo K. (1997). The determination of phosphorus in seawater. In: Bermuda Atlantic Time-series Study Methods, pp 71–74.

539 Michaels A, Dow R, Howse F. (1997). The determination of nitrate in seawater. In: Bermuda
540 Atlantic Time-series Study Methods, pp 61–66.

541 Moore CM, Mills MM, Achterberg EP, Geider RJ, LaRoche J, Lucas MI, et al. (2009). Large-
542 scale distribution of Atlantic nitrogen fixation controlled by iron availability. Nat Geosci **2**: 867–
543 871.

544 Moore CM, Mills MM, Arrigo KR, Berman-Frank I, Bopp L, Boyd PW, et al. (2013). Processes
545 and patterns of oceanic nutrient limitation. Nat Geosci **6**: 701-710. doi:10.1038/ngeo1765.

546 Moore LR, Goericke R, Chisholm S. (1995). Comparative physiology of Synechococcus and
547 Prochlorococcus: influence of light and temperature on the growth, pigments, fluorescence and
548 absorptive properties. Mar Ecol Prog Ser **116**: 259–275.

549 Van Mooy BAS, Rocap G, Fredricks HF, Evans CT, Devol AH. (2006). Sulfolipids dramatically
550 decrease phosphorus demand by picocyanobacteria in oligotrophic marine environments. Proc
551 Natl Acad Sci U S A **103**: 8607–8612.

552 Morel FMM. (1987). Kinetics of nutrient uptake and growth in phytoplankton. J Phycol **23**: 137–
553 150.

554 Mouginot C, Zimmerman AE, Bonachela JA, Fredricks H, Allison SD, Van Mooy BAS, et al.
555 (2015). Resource allocation by the marine cyanobacterium Synechococcus WH8102 in response
556 to different nutrient supply ratios. Limnol Oceanogr **60**: 1634-1641. doi:10.100/lno10123.

557 Pahlow M, Oschlies A. (2009). Chain model of phytoplankton P, N and light colimitation. Mar
558 Ecol Prog Ser **376**: 69–83.

559 Rao NN, Gómez-García MR, Kornberg A. (2009). Inorganic polyphosphate: essential for growth
560 and survival. Annu Rev Biochem **78**: 605–647.

561 Rhee GY. (1978). Effects of N:P atomic ratios nitrate limitation on algal growth, cell
562 composition, nitrate uptake. Limnol Oceanogr **23**: 10–25.

563 Rhee G-Y. (1973). A continuous culture study of phosphate uptake, growth rate, and
564 polyphosphate in Scenedesmus sp. J Phycol **9**: 495–506.

565 Scanlan DJ, Ostrowski M, Mazard S, Dufresne A, Garczarek L, Hess WR, et al. (2009).
566 Ecological genomics of marine picocyanobacteria. Microbiol Mol Biol Rev **73**: 249–299.

567 Schaechter M, MaalOe O, Kjeldgaard NO. (1958). Dependency on medium and temperature of
568 cell size and chemical composition during balanced growth of Salmonella typhimurium. J Gen
569 Microbiol **19**: 592–606.

570 Shuter B. (1979). A model of physiological adaptation in unicellular algae. J Theor Biol **78**: 519–
571 552.

572 Sterner RW, Elser JJ. (2002). Ecological stoichiometry: The biology of elements from molecules
573 to the biosphere. Princeton University Press.

574 Sterner RW, Elser JJ, Fee EJ, Guildford SJ, Chrzanowski TH. (1997). The light: nutrient ratio in
575 lakes: the balance of energy and materials affects ecosystem structure and process. Am Nat **150**:
576 663–684.

577 Teng Y-C, Primeau FW, Moore JK, Lomas MW, Martiny AC. (2014). Global-scale variations of
578 the ratios of carbon to phosphorus in exported marine organic matter. Nat Geosci **7**: 895–898.

Urabe J, Kyle M, Makino W, Yoshida T, Andersen T, Elser JJ. (2002). Reduced light increases herbivore production due to stoichiometric effects of light/nutrient balance. Ecology **83**: 619–627.

Vadia S, Levin PA. (2015). Growth rate and cell size: a re-examination of the growth law. Curr Opin Microbiol **24**: 96–103.

Verspagen JMH, Van de Waal DB, Finke JF, Visser PM, Huisman J. (2014). Contrasting effects of rising CO_2 on primary production and ecological stoichiometry at different nutrient levels. Ecol Lett **17**: 951–960.

Waterbury J, Willey JM. (1988). Isolation and growth of marine planktonic Cyanobacteria. Methods Enzymol **167**: 100–105.

Wingard LL, Miller SR, Sellker JML, Stenn E, Allen MM, Wood a. M. (2002). Cyanophycin production in a phycoerythrin-containing marine Synechococcus strain of unusual phylogenetic affinity. Appl Environ Microbiol **68**: 1772–1777.

Wyman M, Gregory RP, Carr NG. (1985). Novel role for phycoerythrin in a marine cyanobacterium, Synechococcus strain DC2. Science **230**: 818–820.

Yeh SW, Ong LJ, Glazer AN. (1986). Role of phycoerythrin in marine picoplankton Synechococcus spp. **234**: 1422–1423.

Zimmerman AE, Allison SD, Martiny AC. (2014). Phylogenetic constraints on elemental stoichiometry and resource allocation in heterotrophic marine bacteria. Environ Microbiol **16**: 1398-1410. doi:10.1111/1462-2920.12329.

Zimmerman AE, Martiny AC, Lomas MW, Allison SD. (2014). Phosphate supply explains variation in nucleic acid allocation but not C:P stoichiometry in the western North Atlantic. Biogeosciences **11**: 1599–1611.

Figure legends

Figure 1 Interactive influence of growth rate and nutrient supply on cellular quotas of Synechococcus. Cellular carbon (Q_C, a), nitrogen (Q_N, b), and phosphorus (Q_P, c) quotas of Synechococcus as a function of steady-state growth (μ) in chemostat cultures limited by nitrate (open symbols) or phosphate (closed symbols). Data were fitted to the Droop model ($\mu = \mu_\infty \cdot [1 - Q'_{min}/Q]$) for P-limited (solid lines), and N-limited (dashed[a] and dotted[b] lines) cells, where μ is the growth rate, μ_∞ is the conditional maximum growth rate, Q'_{min} is the conditional minimum elemental quota and Q is the elemental quota. Large[a] and small[b] open symbols represent data from independent, N-limited culture trials. Standard deviations are plotted on means of triplicate measurements from the last 3 sampling time points during a trial.

613

614 **Figure 2** Growth-dependent changes in cell size of Synechococcus. Cell size (estimated with a
615 cell carbon to cell volume relationship) (a) and forward scatter (FSCH, a proxy for cell diameter;
616 b) of Synechococcus cells as a function of steady-state growth (μ) in chemostatic cultures limited
617 by nitrate (open symbols) or phosphate (closed symbols). Open circles represent data from two
618 independent, N-limited culture trials. Standard deviations are plotted on means of triplicate
619 measurements from the last 3 sampling time points during a trial.

620

621 **Figure 3** Proportion of cellular nitrogen and phosphorus quotas devoted to nucleic acids.
622 Cellular nitrogen (N, triangles) and phosphorus (P, circles) in total cellular nucleic acids (a),
623 cellular RNA (b) and cellular DNA (c) as a proportion of total cellular N and P, respectively, as a
624 function of steady-state growth (μ) in chemostatic cultures of Synechococcus limited by nitrate
625 (open symbols) or phosphate (closed symbols). Open symbols represent data from two
626 independent, N-limited culture trials. Standard deviations are plotted on means of triplicate
627 measurements from the last 3 sampling time points during a trial.

628

629 **Figure 4** Interactive influence of growth rate and nutrient limitation on cellular stoichiometry of
630 Synechococcus. Cellular elemental ratios of carbon:phosphorus ($C:P_{cell}$, a), nitrogen:phosphorus
631 ($N:P_{cell}$, b) and carbon:nitrogen ($C:N_{cell}$, c) as a function of steady-state growth (μ) in
632 chemostatic cultures of Synechococcus limited by nitrate (open circles, $C:P_{cell}$: $r^2 = 0.65$, slope =
633 -35.7; y-intercept = 150) or phosphate (closed circles; $C:P_{cell}$: $r^2 = 0.97$; slope = -255 y-intercept
634 = 381; $N:P_{cell}$: $p < 0.05$, $r^2 =$; slope = -38.9; y-intercept = 58.6). Open circles represent data from
635 two independent, N-limited culture trials. Hashed symbols where $\mu = 0$ represent calculated

636 ratios from conditional minimum elemental quotas (Q'_{min}) from Droop models in Figure 1.
637 Standard deviations are plotted on means of triplicate measurements from the last 3 sampling
638 time points during a trial. Model output data are also included (see further details in
639 Supplementary Information).
640

641 **Figure 1:**

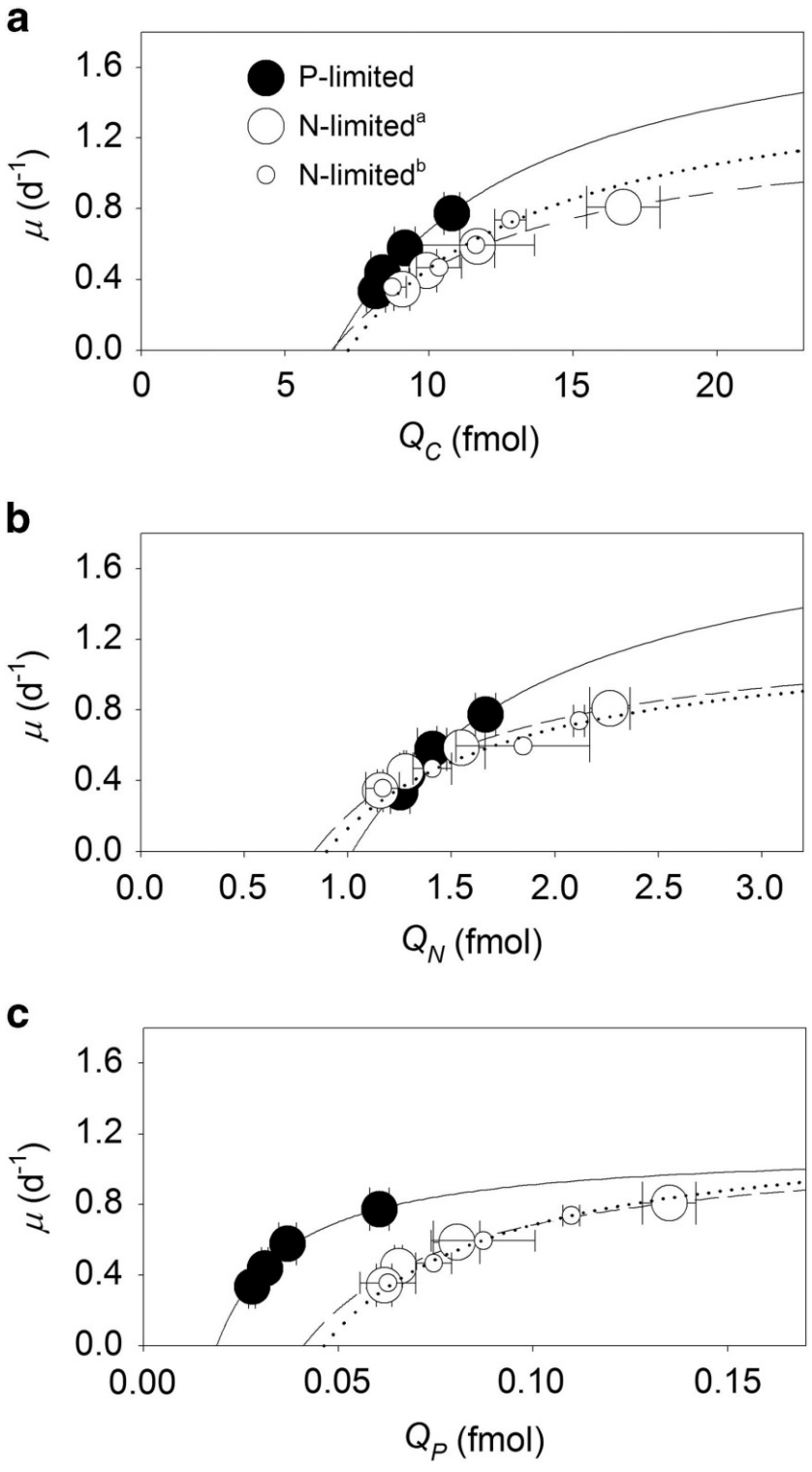

642

643

644 **Figure 2:**

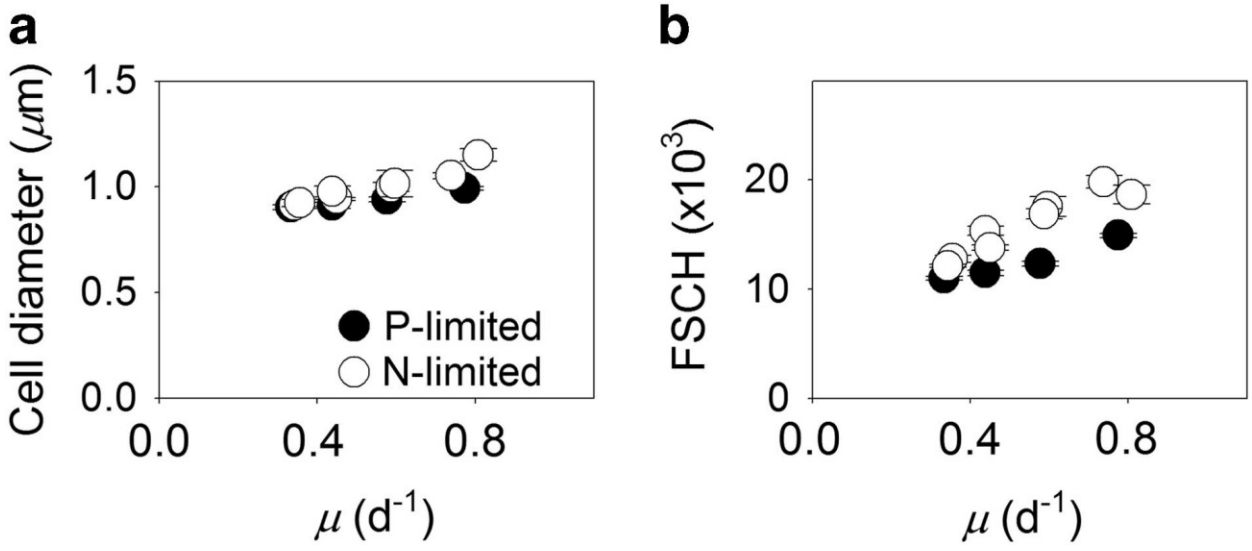

645

646

647 **Figure 3:**

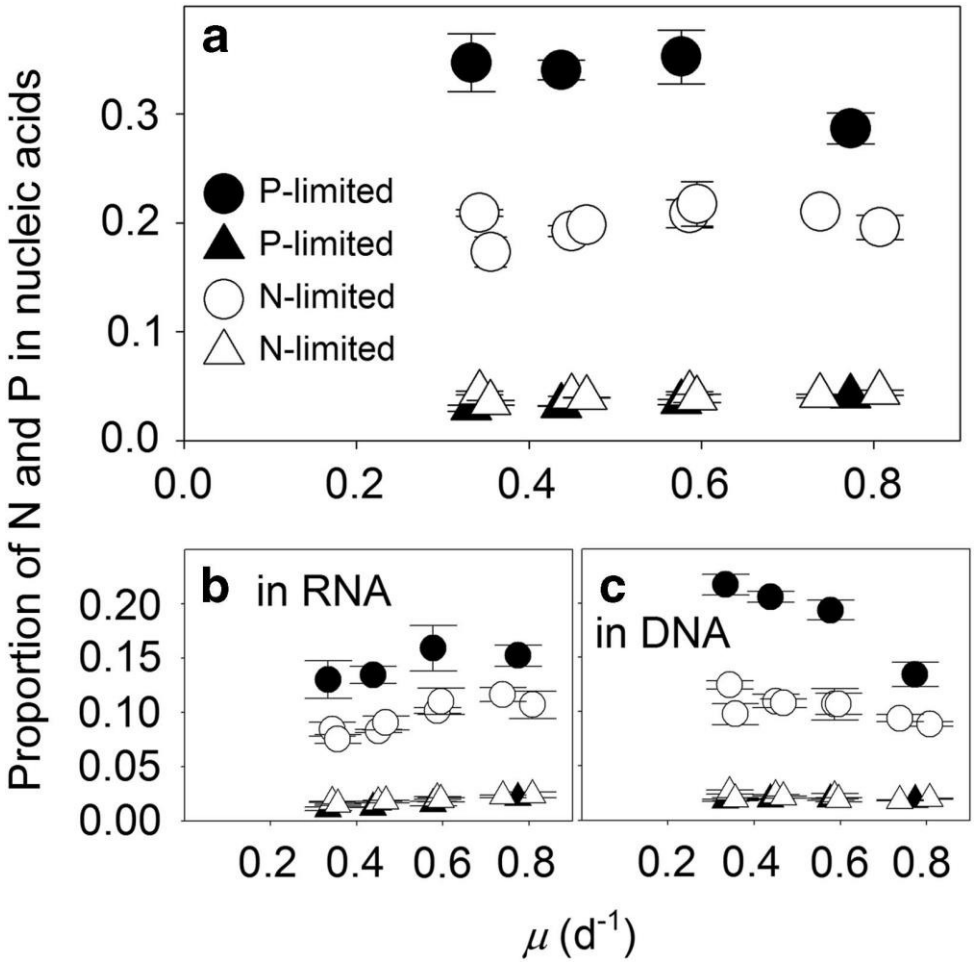

648

649 **Figure 4:**

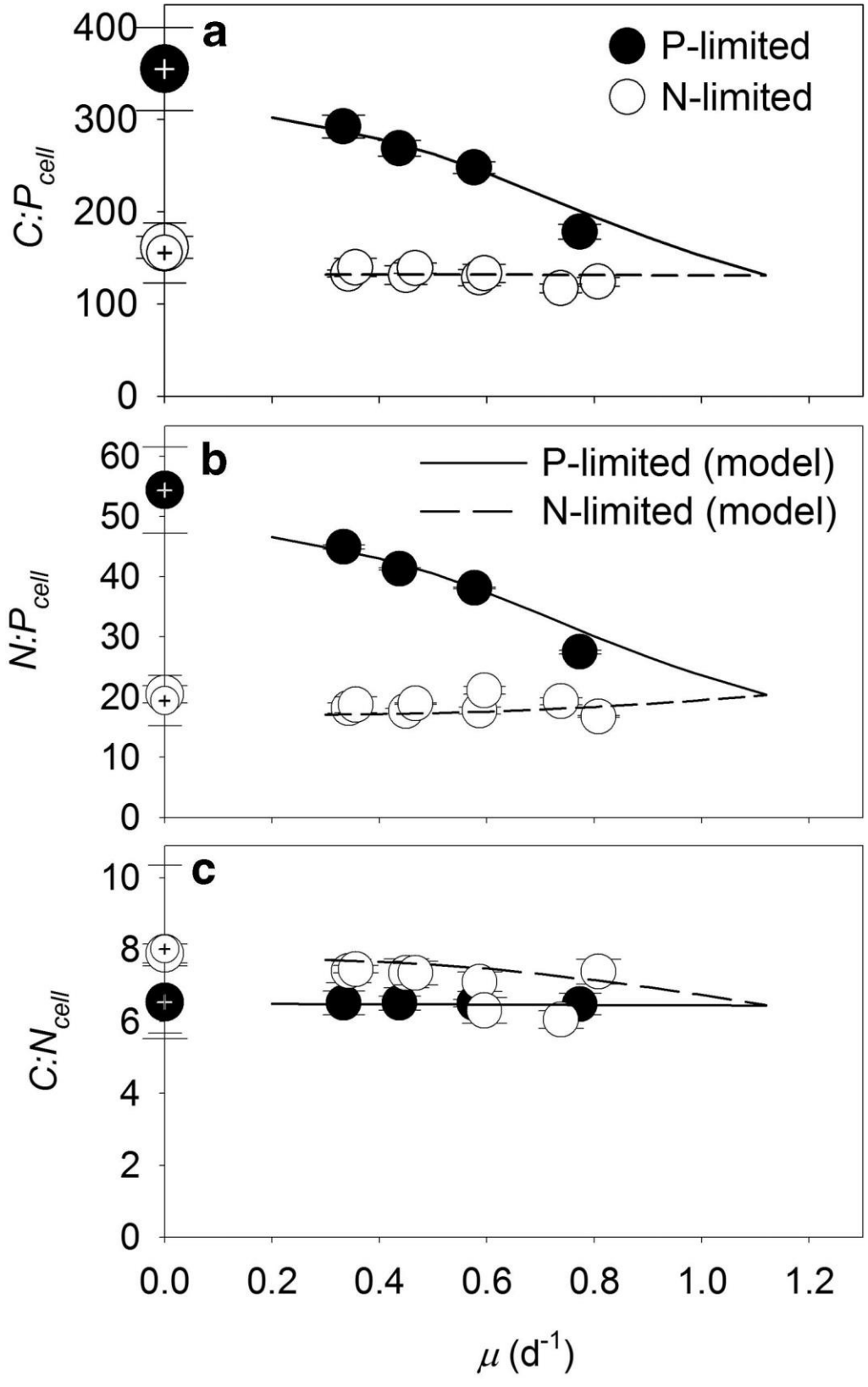

650

651 **Supplementary Information**
652
653 **Elemental ratios under N-limitation**

654 A previous study of elemental stoichiometry suggested that $N:P_{cell}$ was near 10 in slow-
655 growing N-limited cultures (Mouginot et al., 2015), whereas our data indicate the $N:P_{cell}$ was
656 near 18 at a similar growth rate (Figure 4, main text). Although we do not know the reason for
657 this difference, there were several differences between the data and methods that were
658 implemented in these two studies. First, we note that Q_C varied by nearly an order of magnitude
659 in the previous study but was relatively stable in our trials (Supplementary Figure S1). Second,
660 we used an artificial seawater medium, whereas natural seawater was used in the previous study.
661 Third, the methods used for analyzing particulate organic phosphorus were different between
662 these two studies. For example, in the previous study, the method excluded a rinsing technique
663 with a sodium sulfate solution to remove extracellular phosphorus from the analysis of
664 particulate organic phosphorus. Lastly, the total biomass, iron and phosphorus concentrations in
665 chemostat cultures were considerably higher during the previous study, while the light intensity
666 was nearly an order of magnitude lower in comparison with our study.

667 **Model Description**

668 We built on an existing model in order to reproduce the phenomenology presented in the
669 main text. The modifications enabled replicating the observed behavior, which allowed us to
670 identify key biological mechanisms responsible for such behavior.

671 Starting point

672 The model, introduced in Bonachela et al. (2013), keeps track of the dynamics of carbon,
673 C, nitrogen, N, and phosphorus, P, of a generic phytoplankton population. In the present paper,
674 we parametrized the model according to the specific Synechococcus isolate (WH8102) used in

675 our laboratory experiments (see main text and Supplementary Table S2). In addition, we
676 considered chemostat conditions with a dilution rate set by w; thus, the equations for the
677 inorganic N and P concentrations, [N] and [P] respectively, are given by:

$$\frac{d[N]}{dt} = w([N_0] - [N]) - V_N \quad (1)$$

$$\frac{d[P]}{dt} = w([P_0] - [P]) - V_P \quad (2)$$

679 where $[N_0]$ and $[P_0]$ represent the input concentrations, and V_N and V_P represent the population-
680 level uptake, of N and P, respectively.

681 Similarly to the original model, the population-level equations for N and P are simple
682 balance equations given by:

$$\frac{dN}{dt} = V_N - wN \quad (3)$$

$$\frac{dP}{dt} = V_P - wP \quad (4)$$

684 Therefore, the population N and P increase through uptake and decrease due to dilution (washout
685 of individuals). For the sake of simplicity, we consider that any source of exudation or
686 consumption of N and P is negligible when compared with uptake or dilution rates. The
687 population-level uptake rates are given by the equations:

$$V_N(t) = \frac{V_{max_N}[N]}{[N] + \tilde{K}_N} B(t) \quad (5)$$

$$V_P(t) = \frac{V_{max_P}[P]}{[P] + \tilde{K}_P} B(t) \quad (6)$$

where B(t) is the number of cells in the population, V_{maxX} represents the cell-level maximum uptake rate for nutrient X, and $\check{K}_X$ a generalized expression for the half-saturation constant linked to nutrient X given by:

$$\tilde{K}_N = K_N\left(1+\frac{V_{max_N}}{4\pi D_N r_c K_N}\right) \quad (7)$$

$$\tilde{K}_P = K_P\left(1+\frac{V_{max_P}}{4\pi D_P r_c K_P}\right) \quad (8)$$

where K_X is the standard half-saturation constants associated with the uptake of nutrient X, D_X is the diffusivity of the element in the medium, and r_c is the cell radius. Note that this generalized expression for the half-saturation constant is affected by changes in V_{maxX} (for instance, when resource availability changes), which allows the uptake rate expressions above (Eqs.5 and 6) to show well-known extreme cases (diffusion- versus handling-limitation uptake rates) (Bonachela et al., 2011).

Also similarly to the original model, we consider here the possibility for the phytoplankton cell to alter the number of proteins used to take up the different nutrients. This number of proteins is linked to the maximum uptake rate; if n_X is the number of uptake proteins for nutrient X in the population (Bonachela et al., 2011):

$$V_{max_X} = k_{2_X} n_X(t)/\left(B(t)N_A\right) \quad (9)$$

where N_A is Avogadro's number, and k_{2X} is the nutrient ion handling rate:

$$k_{2_X} = 4D_X r_c K_X N_A \quad (10)$$

To establish the dynamics of this number of proteins, we define the expression function, F, and the repression function, G. The expression function represents the synthesis strategy of the cell, i.e. whether to produce uptake proteins for nutrient X, according to the internal content of

such nutrient, Q_X (nutrient quota; Droop, 1968). Specifically, if the quota is low (close to the minimum required to grow, Q_{min}), the cell upregulates the synthesis of proteins to compensate for the lack of the limiting nutrient by increasing its maximum uptake rate and, therefore, the probability of acquiring a nutrient when the cell encounters that nutrient; on the other hand, if the quota is close to the maximum that the cell can store, Q_{max}, synthesis is downregulated to save maintenance and synthesis energy that can be thus allocated to growth. This behavior, which has been theoretically justified and experimentally shown in the past (Dyhrman and Palenik, 2001; Morel, 1987) can be encoded using the following functional form (Bonachela et al., 2011):

$$F\left(\frac{Q_{max}-Q}{Q_{max}-Q_{min}}\right)=\frac{2}{1+e^{-k_F\left(\frac{Q_{max}-Q}{Q_{max}-Q_{min}}\right)}}-1, \tag{11}$$

where k_F is a shape factor. Similarly, the repression function sets a constraint for this strategy according to the availability of ribosomes, responsible for protein synthesis. Ribosomes are phosphorus-rich; therefore, the lower the P quota, the smaller the repression function is, thus limiting protein synthesis (Bonachela et al., 2013):

$$G\left(\frac{Q_P-Q_{P_{min}}}{Q_{P_{max}}-Q_{P_{min}}}\right)=\frac{1}{1+e^{-k_{G,1}\left(\frac{Q_P-Q_{P_{min}}}{Q_{P_{max}}-Q_{P_{min}}}-k_{G,2}\right)}}, \tag{12}$$

where $k_{G,1}$ and $k_{G,2}$ are factors that shape the exponential function.

With the elements above, the dynamics for the number of N-uptake proteins, n_N, and the dynamics for the number of P-uptake proteins, n_P , is given by:

$$\frac{dn_N}{dt}=\nu_N H\left(1-A_{rel}(t)\right)F\left(\frac{Q_{N_{max}}-Q_N(t)}{Q_{N_{max}}-Q_{N_{min}}}\right)G\left(\frac{Q_P(t)-Q_{P_{min}}}{Q_{P_{max}}-Q_{P_{min}}}\right)B(t)-wn_N(t), \tag{13}$$

$$\frac{dn_P}{dt} = \nu_P H\left(1 - A_{rel}(t)\right) F\left(\frac{Q_{P_{max}} - Q_P(t)}{Q_{P_{max}} - Q_{P_{min}}}\right) G\left(\frac{Q_P(t) - Q_{P_{min}}}{Q_{P_{max}} - Q_{P_{min}}}\right) B(t) - wn_P(t), \quad (14)$$

where ν_X is the maximum synthesis rate per cell and unit time, and H is a Heaviside function that represents the physical impossibility for cells to store more uptake proteins beyond their total surface area (A_{rel} is the ratio absorbing to total area, assuming circular transporter and cell surfaces).

Note that the equations above transform V_{max} into a dynamic variable that responds to the whole nutritional history of the cell. Importantly, through this dependence on the past and present values of the cell quota, the cell develops a link between V_{max} and the external nutrient concentration that allows the generalized expressions for the uptake rates above, Eqs.5 and 6, to show the two well-known extreme cases mentioned above, i.e. diffusion limitation (when V_{max} is large, which occurs when the focal nutrient concentration is low), and handling-limitation (when V_{max} is small, which occurs when the focal nutrient concentration is large). See (Bonachela et al., 2011, 2013) and references therein for more detailed information about the deduction of all these expressions and functions.

Different from the original model, the variability observed in the per-cell C content (or C quota, Q_c) makes it necessary for the model to separately keep track of the dynamics of C and the number of cells in the population, B (Bonachela et al., 2013). With such a dynamic approach, the stationary value for Q_c shown by the cell emerges from the mechanisms considered in the model, as opposed to imposing a Droop-like dependence for Q_c on the dilution rate, w.

The equation for the population-level C is also a balance equation that considers photosynthesis as the only source of organic carbon, and respiration and dilution as the only negative terms contributing to the decrease of such organic carbon. Following similar reasoning to that of the

uptake protein dynamics, photosynthetic proteins are dynamically regulated, and the production strategy depends on the availability of carbon (through the expression function) and is constrained by the availability of both nitrogen and phosphorus (through the repression function). On the other hand, we considered the carbon-based uptake rates for N and P as main sources of carbon respiration for the cell (Geider et al., 1998). Thus, the equation for C is given by:

$$\frac{dC}{dt} = \left[P_{max}\, F\left(\frac{Q_{C_{max}} - Q_C(t)}{Q_{C_{max}} - Q_{C_{min}}} \right) G\left(\frac{Q_N(t) - Q_{N_{min}}}{Q_{N_{max}} - Q_{N_{min}}} \right) G\left(\frac{Q_P(t) - Q_{P_{min}}}{Q_{P_{max}} - Q_{P_{min}}} \right) - M_{C,N}\frac{V_N}{C} - M_{C,P}\frac{V_P}{C} - w \right] C, \quad (15)$$

where P_{max} is the maximum photosynthetic rate and $M_{C,N}$ and $M_{C,P}$ are respiration rates. In addition, the equation for the number of cells in the population is given by (Lehman et al., 1975):

$$\frac{dB}{dt} = \left[f(Q_C, Q_N, Q_P) - w \right] B(t), \quad (16)$$

where f is an increasing function of the quotas of the focal elements. Thus, the more C, N, and P, the more individuals are created in the population. For the results presented here, we used the function:

$$f(Q_C, Q_N, Q_P) = \mu_\infty \left[\left(\frac{Q_C(t) - Q_{C_{min}}}{Q_{C_{max}} - Q_{C_{min}}} \right) \left(\frac{Q_N(t) - Q_{N_{min}}}{Q_{N_{max}} - Q_{N_{min}}} \right) \left(\frac{Q_P(t) - Q_{P_{min}}}{Q_{P_{max}} - Q_{P_{min}}} \right) \right]^b, \quad (17)$$

with b = 0.5 but, as discussed in the next section, other functional forms could also reproduce the experimental data in a similar way.

Parametrization

In order to obtain the results presented in the next section, we used a parametrization that combined data from the literature and information we collected in the laboratory. On one hand, respiration, maximum photosynthetic and biosynthetic rates, diffusivity constants, half-saturation

761 constants were all set to fixed values obtained from the existing experimental and/or modeling
762 literature for Synechococcus (Supplementary Table S2).
763
764 On the other hand, crucial parameter values such as the physiological limits for the quotas were
765 deduced from our laboratory observations. For example, Fig. S6 shows that the volume-
766 normalized N quota remains constant as dilution rate increases when P is limiting; reciprocally,
767 the volume-normalized P quota shows a slightly increasing behavior when N is limiting. Thus,
768 we interpreted this lack of dependence on the dilution rate as an indication that these quotas have
769 reached their maximum values. Therefore, if V_c represents cell volume, we can deduce that:

$$\begin{aligned} Q_{N_{max}} &\sim 3.25\times10^{-15}V_c, \\ Q_{P_{max}} &\sim 0.16\times10^{-15}V_c. \end{aligned} \tag{18}$$

770 In addition, and according to the data in table 1 (main text), we can deduce a dependence
771 between the minimum values for the N and P quotas for the three different experiments, and the
772 value of Q_c shown by the cell when those minima were reached. This calculation provides a
773 rough estimate for the minimum quotas given by:

$$\begin{aligned} Q_{N_{min}} &\sim 0.126\times Q_C, \\ Q_{P_{min}} &\sim 2.790\times10^{-3}Q_C. \end{aligned} \tag{19}$$

774 In turn, we assume that cell volume and carbon quota are linked through the Synechococcus-
775 specific expression (Heldal et al., 2003):

$$V_c = 0.004\left(12\times10^{15}Q_C\right) - 0.0045 \tag{20}$$

776 which determines the cell radius, r_c, assuming spherical cells. Note that, because Q_c changes
777 dynamically (see above), the physiological limits for the N and P quotas will also change
778 throughout each numerical experiment.

779 Regarding the limits for the carbon quota, Fig.1 in the main text shows that Q_{Cmin} does not
780 depend on environmental conditions. The maximum value for Q_c, on the other hand, should be
781 set by growth requirements and, therefore, Q_{Cmax} should depend on the cell's growth rate. A naive
782 argument that can provide such dependence is that the maximum quota should scale with cell
783 volume; additionally, our own observations show that cell radius is linearly related with the
784 dilution rate (see Figure 2, main text). Thus, and considering the fact that Q_{Cmax} necessarily needs
785 to be equal to or larger than any of the values for Q_c collected in our experiments:

$$Q_{C_{max}} \sim 16\times10^{-15}\left(\frac{\mu}{\mu_\infty}\right)^3 + Q_{C_{min}}. \quad (21)$$

786 In the next section, we present the results obtained with the model, as well as a brief discussion
787 about other possible choices for some of the terms presented here.

788 Model Output

789 With the model above, the emergent trends in phytoplankton stoichiometry are very close to
790 those obtained in the laboratory (see Figure 4, main text).

791 In order to obtain the almost total lack of dependence of $C:P_{cell}$, $N:P_{cell}$, and $C:N_{cell}$ on growth
792 rate when N is limiting (Figure 4, main text), it was a necessary condition for both, $V_{max,N}$ and
793 $V_{max,P}$,to depend on the quotas. Constant V_{max} such as the ones provided in the classic Michaelis-
794 Menten formulation of uptake rates, which simpler models assume (Legović and Cruzado, 1997;
795 Klausmeier et al. 2004a; Klausmeier et al., 2004b), would provide such constant behavior only
796 when the input ratio is close to the so-called optimal ratio; the closeness of the quotas to their

797 maximum levels in our experiments indicates that cells are, however, far from such optimal
798 point. In our case, the mechanistic equations Eq.13 and Eq.14 provide the necessary link between
799 maximum uptake rates and internal elemental quotas. Phenomenological models (e.g. 11, 12) can
800 potentially provide similar results, because we are describing stationary states and thus the
801 dynamics of V_{max} are not key to the observed behavior, but the mentioned emergent dependence
802 between V_{max} and the quotas.

803 The model was qualitatively insensitive to using in Eq. 21 the constant value of the dilution
804 rate, w, instead of the growth rate. Additionally, the specific form of the function f in Eq. 16
805 affects significantly C:P when P is limiting. This function determines B, and therefore influences
806 the behavior of the quotas. Values of the exponent $b = 0.5 \pm 0.15$ still provide satisfactory
807 replication of the data. Similarly, assuming a combination of Droop-like terms such as:

$$f(Q_C, Q_N, Q_P) = \mu_\infty \left[\left(\frac{1 - Q_{C_{min}}/Q_C(t)}{1 - Q_{C_{min}}/Q_{C_{max}}} \right) \left(\frac{1 - Q_{N_{min}}/Q_N(t)}{1 - Q_{N_{min}}/Q_{N_{max}}} \right) \left(\frac{1 - Q_{P_{min}}/Q_P(t)}{1 - Q_{P_{min}}/Q_{P_{max}}} \right) \right] \quad (22)$$

808 can also produce satisfactory results. Other forms that also replicate the experimental data
809 include terms assuming Liebig's law of the minimum, i.e. f functions that depend only on the
810 most limiting nutrient by means of Droop-like terms or square-root terms as the ones proposed
811 above (results not shown):

$$f(Q_C, Q_N, Q_P) = \mu_\infty \min \left[\left(\frac{1 - Q_{C_{min}}/Q_C(t)}{1 - Q_{C_{min}}/Q_{C_{max}}} \right), \left(\frac{1 - Q_{N_{min}}/Q_N(t)}{1 - Q_{N_{min}}/Q_{N_{max}}} \right), \left(\frac{1 - Q_{P_{min}}/Q_P(t)}{1 - Q_{P_{min}}/Q_{P_{max}}} \right) \right]. \quad (23)$$

812 Thus, we can deduce that another necessary mechanism that determines how the cell's
813 stoichiometry reacts to changes in its growth rate is a dependence of the population density on
814 the quotas following a functional form that scales faster than linearly with the cell quota.

In order to replicate the quota behavior observed in the laboratory (Figure 1, main text), it was also essential for the model to consider a dilution-rate-dependent Q_c, as such dependence affects directly the scaling relationships Eqs.19 and 20. In our case, we used a dynamic equation that allows that dependence to emerge from the cell's own regulation, Eq.15. Alternatively, a data-deduced Q_c curve that provides such dependence would suffice to provide the necessary dependence of the physiological limits on the cell's stationary growth rate (results not shown).

Finally, as shown in Figs.1 and S7, our model replicates P-limited quotas more closely than N-limited quotas. The reason is that our equation for Q_C does not distinguish between P- and N-limited cells, and provides an emergent Q_C that is numerically closer to the P-limited carbon quota than to the N-limited one (Figure 1a, main text). Ultimately, this lack of dependence of Q_C on which nutrient is limiting results from the proximity of the emergent Q_C to Q_{Cmax}, and the use of the same Q_{Cmax} expression (Eq.21) for both N- and P-limiting cases. Tailoring Eq.21 to P-limited and N-limited cells (e.g. by adjusting the maximum growth rate) will bring model data closer to observational data, at the expense of losing generality and simplicity.

We can quantify the effect of the mechanisms mentioned above by measuring the relative distance to observations obtained with our model, and obtained with a version of the model in which either cell size or both V_{max} are held constant. For the former, we tried the obvious choice of cell diameter around the average observed in our experiments across dilution rates (~1 μm), but the maximum cell diameter observed (~1.2 μm) actually provided better estimates for elemental ratios (Supplementary Figure S7). For the latter, we used the allometric relationships for $V_{max,N}$ and $V_{max,P}$ deduced from data compilations in Edwards et al. (2012) together with the variable cell size described in our model (data not shown), or a fixed value for the maximum

838 uptake rates deduced from the allometries using a cell diameter around 1.2 μm (Supplementary
839 Figure S7). As shown in Supplementary Figure S7A, fixing the cell size barely influences the
840 N:P ratio. However, it influences deeply the qualitative behavior of the carbon-related ratios,
841 which show a non-monotonous behavior that differs from our observations (Supplementary
842 Figure S7B and C). Fixing both V_{max} has important qualitative and quantitative impact upon the
843 ratios, which diverge considerably from our observations. Importantly, none of these two
844 variants can replicate the observed quotas (see Supplementary Figure S7D for our model and the
845 fixed-size variant). Note that the performance of the fixed-size version is greatly improved for
846 high growth rates because the chosen fixed size is close to the cell size observed for high growth
847 rates; thus, the difference with observations is greatly reduced by using a growth-dependent cell
848 size (e.g. the emergent dependence included in our model). Our model shows the largest
849 divergence with data precisely for high growth rates at the N-limited case which results, as
850 discussed above, from the nutrient-limitation-generic parametrization we used.

851

852

Table S1. Chemical constituents and concentrations in stock solutions and the growth medium used in chemostat cultures of Synechococcus.

	Kg to 50L	Stock (M)	Medium (M)
Salts			
NaCl	1.08		
$MgSO_4 \cdot 7H_2O$	3.69×10^{-1}		
$MgCl_2 \cdot 6H_2O$	2.04×10^{-1}		
$CaCl_2 \cdot 2H_2O$	7.35×10^{-2}		
KCl	3.75×10^{-2}		
Carbonates			
$NaHCO_3$		1.00	2.00×10^{-3}
Na_2CO_3		3.77×10^{-3}	1.89×10^{-4}
Iron-EDTA solution			
EDTA		1.00×10^{-2}	5.00×10^{-3}
$FeCl_3 \cdot 6H_2O$		1.00×10^{-3}	5.00×10^{-7}
Trace metal solution			
$MnCl_2 \cdot 4H_2O$		14.2×10^{-3}	7.08×10^{-6}
$Na_2MoO_4 \cdot 2H_2O$		3.22×10^{-3}	1.61×10^{-6}
$ZnSO_4 \cdot 7H_2O$		15.4×10^{-4}	7.72x10-7
$CoCl \cdot 6H_2O$		17.18×10^{-5}	8.59×10^{-8}
P-limited cultures			
$NaNO_3$		7.6 x x 10^{-1}	3.8×10^{-5}
KH_2PO_4		11.0×10^{-3}	5.56×10^{-7}
$N:P_{input}$			68.5
N-limited cultures			
$NaNO_3$		3.18×10^{-1}	1.59×10^{-5}
KH_2PO_4		1.84×10^{-1}	9.2×10^{-6}
$N:P_{input}$			1.73

853

854

Table S2. List of variables and parameters used in the model from Synechococcus (Healey, 1985; Hense and Beckmann, 2006; Ikeya et al., 1997; Pahlow and Oschlies, 2009; Flynn et al., 2010).

Symbol	Description	Units	Value
[N]	Dissolved inorganic nitrogen concentration	$mol \cdot l^{-1}$	Variable
[P]	Dissolved inorganic phosphorus concentration	$mol \cdot l^{-1}$	Variable
$[N_0]$	Dissolved inorganic nitrogen supply concentration	$mol \cdot l^{-1}$	$15.9 \cdot 10^{-6}$, $38 \cdot 10^{-6}$
$[P_0]$	Dissolved inorganic phosphorus supply concentration	$mol \cdot l^{-1}$	$9.2 \cdot 10^{-6}$, $0.55 \cdot 10^{-6}$
D_N	Nitrogen diffusion constant in water	$m^2 \cdot d^{-1}$	$1.296 \cdot 10^{-4}$
D_P	Phosphorus diffusion constant in water	$m^2 \cdot d^{-1}$	$8.64 \cdot 10^{-5}$
w	chemostat dilution rate	d^{-1}	0.2-1.2
C	Population (organic) carbon concentration	$mol \cdot l^{-1}$	Variable
N	Population (organic) nitrogen concentration	$mol \cdot l^{-1}$	Variable
P	Population (organic) phosphorus concentration	$mol \cdot l^{-1}$	Variable
B	Number of cells in chemostat	cells	Variable
μ	Population growth rate	d^{-1}	Variable
μ_{max}	Maximum population growth rate	d^{-1}	Emergent
μ_∞	Maximum population growth rate	d^{-1}	1.2
V_N	Population N-uptake rate	$mol \cdot l^{-1} \cdot d^{-1}$	Variable
V_P	Population P-uptake rate	$mol \cdot l^{-1} \cdot d^{-1}$	Variable
V_{maxN}	Maximum cell N-uptake rate	$mol \cdot cell \cdot l^{-1} \cdot d^{-1}$	Variable
V_{maxP}	Maximum cell P-uptake rate	$mol \cdot cell \cdot l^{-1} \cdot d^{-1}$	Variable
K_N	Half-saturation constant for N	$mol \cdot l^{-1}$	$0.3 \cdot 10^{-6}$
K_P	Half-saturation constant for P	$mol \cdot l^{-1}$	$10 \cdot 10^{-9}$
K_N	Diffusion-limited-corrected half-saturation constant for N	$mol \cdot l^{-1}$	Variable
K_P	Diffusion-limited-corrected half-saturation constant for P	$mol \cdot l^{-1}$	Variable
Q_N	Nitrogen cell quota	$mol \cdot cell^{-1}$	Variable
Q_P	Phosphorus cell quota	$mol \cdot cell^{-1}$	Variable
Q_{Nmax}	Maximum N quota	$mol \cdot cell^{-1}$	Variable
Q_{Nmin}	Minimum N quota	$mol \cdot cell^{-1}$	Variable
Q_{Pmax}	Maximum P quota	$mol \cdot cell^{-1}$	Variable
Q_{Pmin}	Minimum P quota	$mol \cdot cell^{-1}$	Variable
Q_C	Carbon content per cell	$mol \cdot cell^{-1}$	Variable
k_{2N}	Handling rate for N	d^{-1}	From Eq. (10)

k_{2P}	Handling rate for P	d^{-1}	From Eq. (10)	
v_N	Maximum N-uptake sites synthesis rate	sites·cell^{-1}·d^{-1}	$\cdot 10^4$	
v_P	Maximum P-uptake sites synthesis rate	sites·cell^{-1}·d^{-1}	$\cdot 10^4$	
A_{rel}	Ratio absorbing:total area	-	Variable	
r_c	Cell radius	m	Variable	
r_s	Uptake site radius	m	$2.5 \cdot 10^{-9}$	
P_{max}	Maximum photosynthetic rate	d^{-1}		5
$M_{C,N}$	Uptake maintenance cost	molC·molN^{-1}		2
$M_{C,P}$	Uptake maintenance cost	molC·molN^{-1}		2
F	Protein expression function	-	Variable	
G	Protein repression function	-	Variable	
H	Heaviside (or step) function	-	Variable	
k_F	Sigmoid slope parameter for F	-		10
$k_{G,1}$	Sigmoid slope parameter for G	-		40
$k_{G,2}$	Sigmoid slope parameter for G	-		0.25
N_A	Avogadro's number	Units·mol^{-1}	$6.02 \cdot 10^{23}$	

855
856

Figure S1. Culture cell density (a-c), forward scatter (FSCH; d-f) and particulate organic carbon (POC; g-i) of Synechococcus cells as a function of steady-state growth (μ) in chemostatic cultures limited by nitrate or phosphate.

Figure S2. Mass balance of nitrogen (a,c) and phosphorus (b,d) in P-limited (a,b) and N-limited (c-f) steady-state chemostatic cultures of Synechococcus. Input nitrate (NO_3^-) and phosphate (PO_4^{3-}) concentrations were measured and indicated with arrows (right of plots) and are close to the summed values of particulate organic nitrogen (PON) or phosphorus (POP) and residual nitrate or phosphate concentrations in cultures. Standard deviations are plotted on means of triplicate measurements from the last 3 sampling time points during a trial.

Figure S3. Cellular elemental ratios of carbon:phosphorus ($C:P_{cell}$) and nitrogen:phosphorus ($N:P_{cell}$) in P-limited (a,b) and N-limited (c-f) chemostatic cultures of Synechococcus diluted at various rates (d^{-1}) during trials (days). Data collected from the last 3 time points during a trial were used to report statistical data in Table 1 and Figures 1-4, S1, S3 and S4. Trial data in panels c and d are independent from trial data in panels e and f.

Figure S4. Cellular elemental quotas of carbon (Q_C, a), nitrogen (Q_N, b), and phosphorus (Q_P, c) as a function of forward scatter (FSCH, a proxy for cell diameter) in steady-state, chemostatic cultures of Synechococcus limited by phosphate (closed symbols) and nitrate (open symbols). Diamonds, squares, triangles, and circles represent data from cultures growing within the ranges of 0.33-0.36 d^{-1}, 0.43-0.47 d^{-1}, 0.57-0.60 d^{-1}, and 0.73-0.81 d^{-1}, respectively. Duplicate open

879 symbols represent independent, N-limited culture trials. Standard deviations are plotted on
880 means of triplicate measurements from the last 3 sampling time points during a trial.
881
882 Figure S5. Cellular deoxyribonucleic acid (DNA_{cell}, a) and ribonucleic acid (RNA_{cell}, b) and
883 fluorescence of pigments Chl a (c) and phycoerythrin (d) as a function of forward scatter (FSCH,
884 a proxy for cell diameter) in steady-state, chemostatic cultures of Synechococcus limited by
885 phosphate (closed symbols) or nitrate (open symbols). Diamonds, squares, triangles, and circles
886 represent data from cultures growing within the ranges of 0.33-0.36 d^{-1}, 0.43-0.47 d^{-1}, 0.57-0.60
887 d^{-1}, and 0.73-0.81 d^{-1}, respectively. Duplicate open symbols represent independent, N-limited
888 culture trials. Standard deviations are plotted on means of triplicate measurements from the last 3
889 sampling time points during a trial.
890
891 Figure S6. Cellular concentration of phosphorus and nitrogen in steady-state, chemostatic
892 cultures of Synechococcus limited by phosphate (closed symbols) and nitrate (open symbols).
893 Standard deviations are plotted on means of triplicate measurements from the last 3 sampling
894 time points during a trial.
895
896 Figure S7. Comparisons between predicted cellular elemental ratios (a-c) using our new model
897 with growth-dependent variation in cell size for P- and N-limited cells of Synechococcus and our
898 model with a fixed cell size or a fixed V_{max}. (d) The percent error between observed elemental
899 quotas and those predicted by our new model is smaller than the percent error between the
900 observed data and our model with a with fixed cell size (d).
901
902

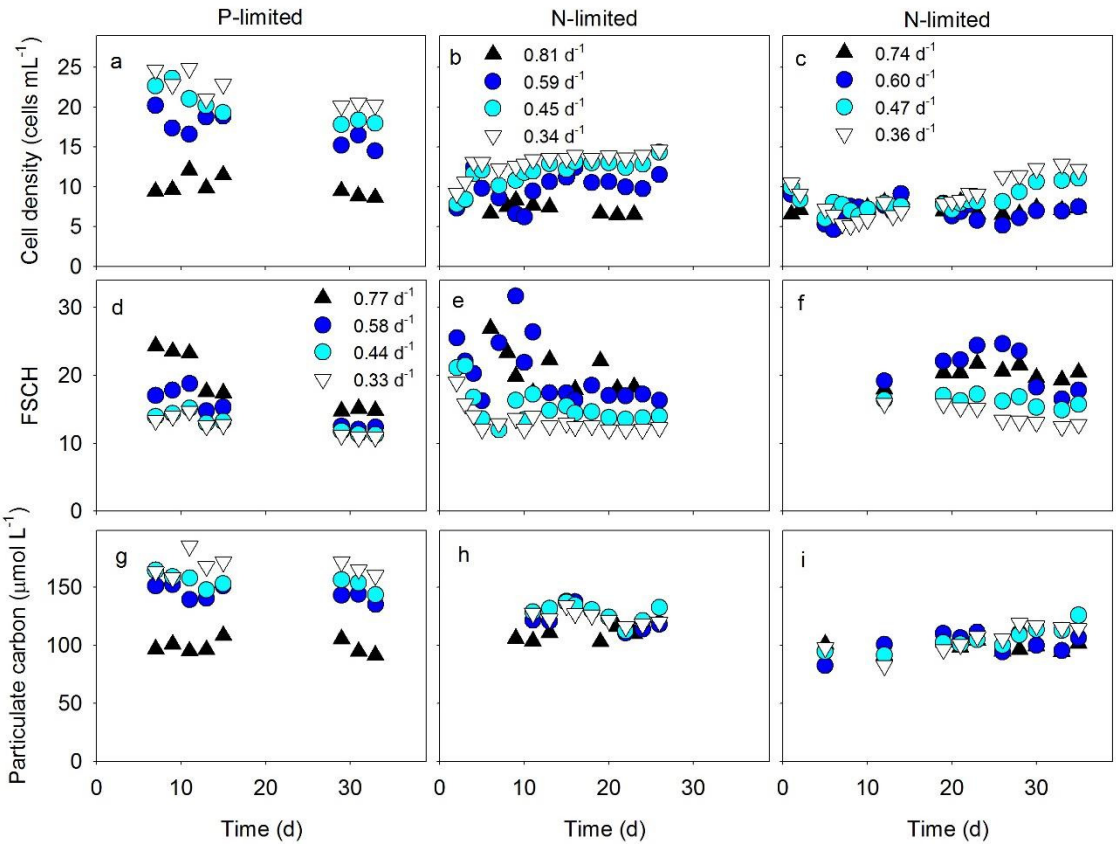
P-limited
N-limited
N-limited
a
b
c
d
e
f
g
h
i
0.81 d-1
0.59 d-1
0.45 d-1
0.34 d-1
0.74 d-1
0.60 d-1
0.47 d-1
0.36 d-1
0.77 d-1
0.58 d-1
0.44 d-1
0.33 d-1
Cell density (cells mL-1)
FSCH
Particulate carbon (µmol L-1)
Time (d)
Time (d)
Time (d)

Figure S1.

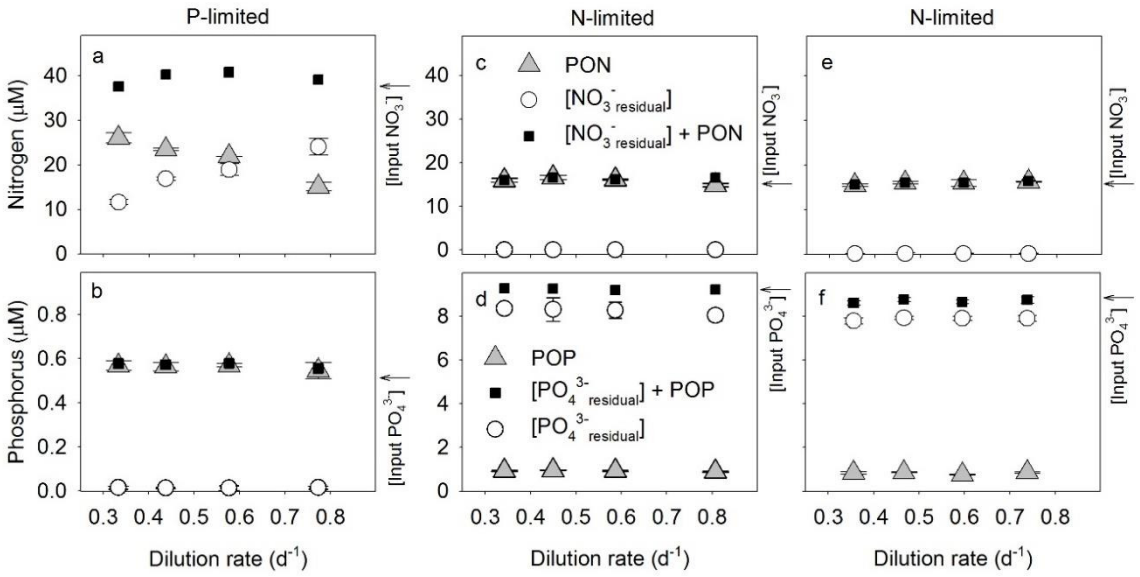

906

907 Figure S2.

908

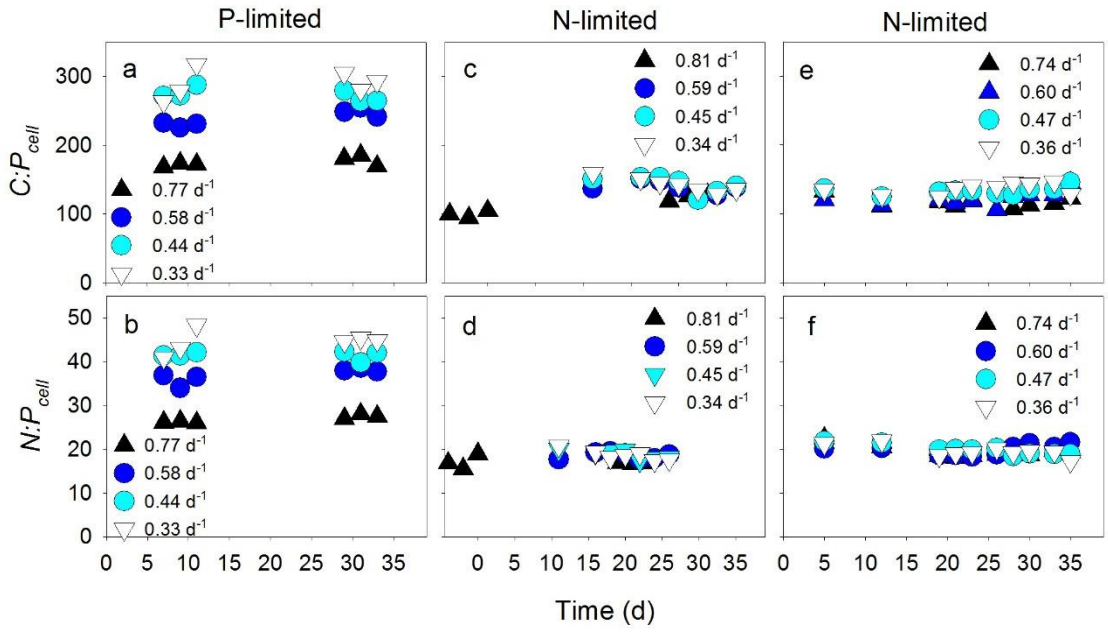

909

910 Figure S3.

911

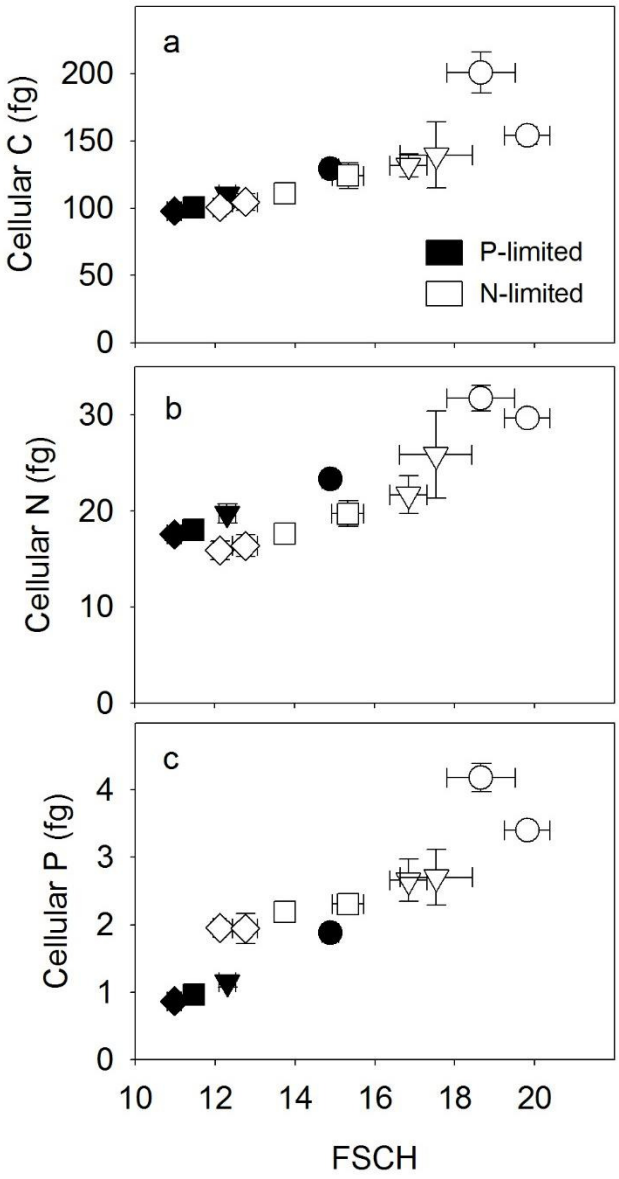

912

913 Figure S4.

914

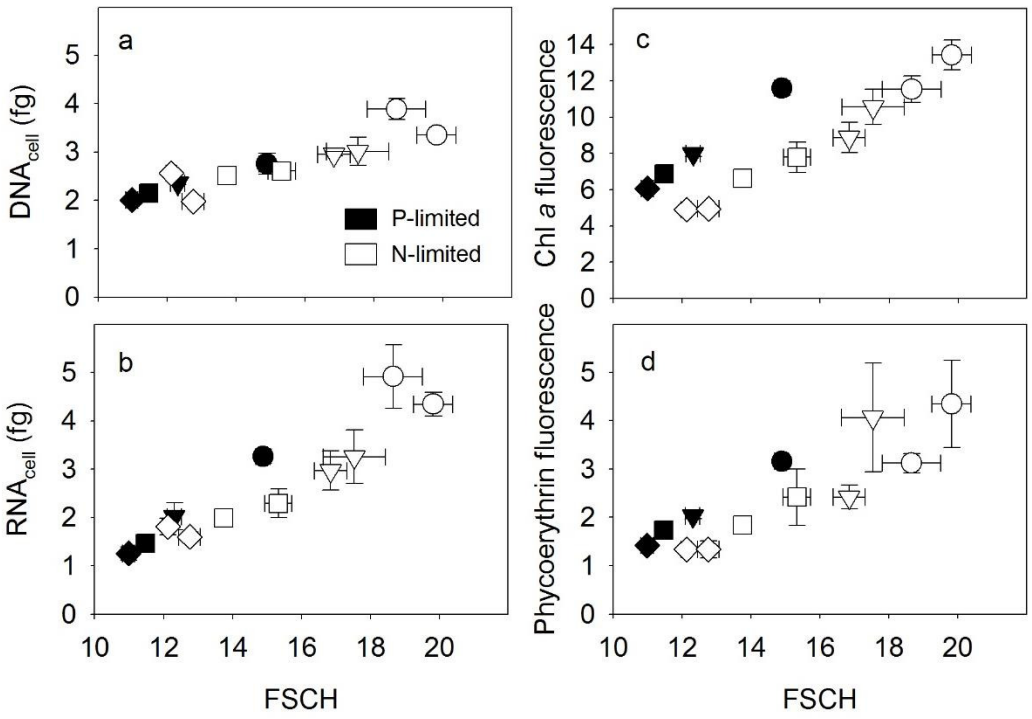

915

916 Figure S5.

917

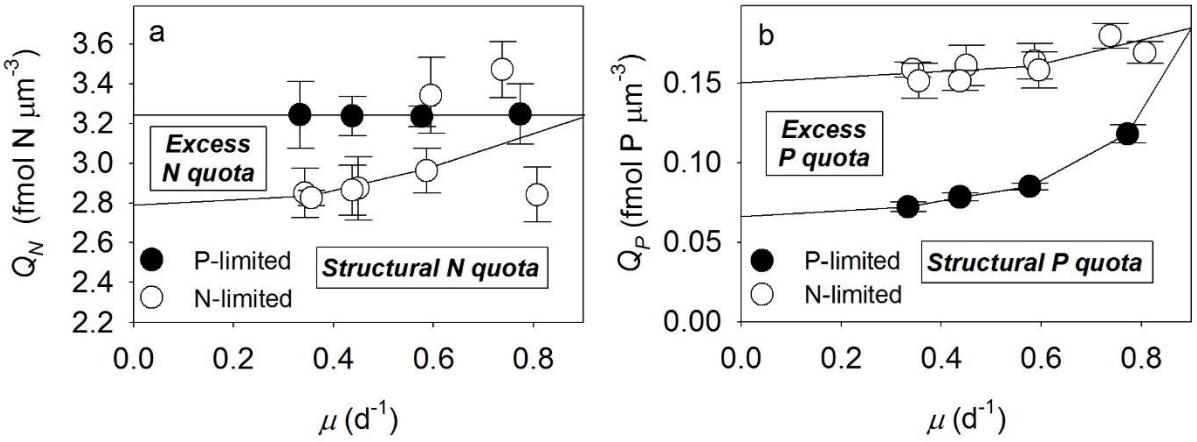
a
b
Excess
N quota
Structural N quota
Excess
P quota
Structural P quota
P-limited
N-limited
Q_N (fmol N µm^{-3})
Q_P (fmol P µm^{-3})
μ (d^{-1})
μ (d^{-1})

Figure S6.

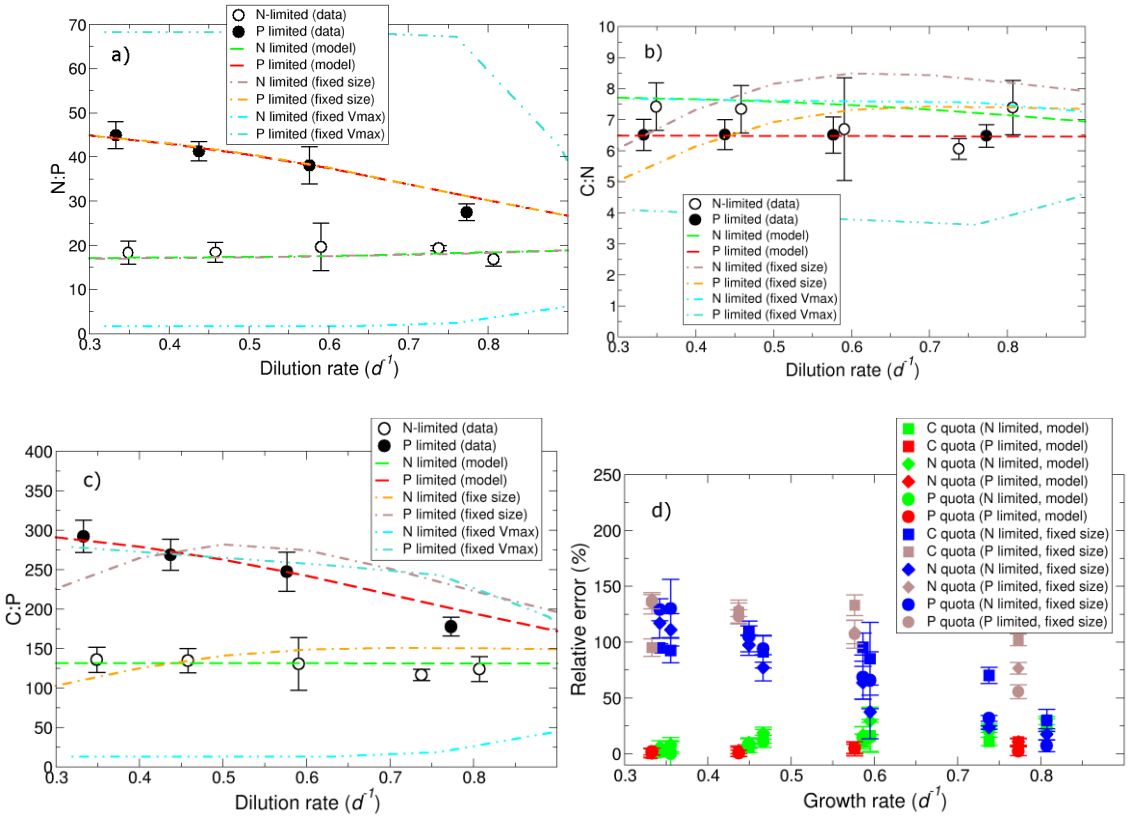
a)
N:P
Dilution rate (d^{-1})
N-limited (data)
P limited (data)
N limited (model)
P limited (model)
N limited (fixed size)
P limited (fixed size)
N limited (fixed Vmax)
P limited (fixed Vmax)
b)
C:N
Dilution rate (d^{-1})
c)
C:P
Dilution rate (d^{-1})
N-limited (data)
P limited (data)
N limited (model)
P limited (model)
N limited (fixe size)
P limited (fixed size)
N limited (fixed Vmax)
P limited (fixed Vmax)
d)
Relative error (%)
Growth rate (d^{-1})
C quota (N limited, model)
C quota (P limited, model)
N quota (N limited, model)
N quota (P limited, model)
P quota (N limited, model)
P quota (P limited, model)
C quota (N limited, fixed size)
C quota (P limited, fixed size)
N quota (N limited, fixed size)
N quota (P limited, fixed size)
P quota (N limited, fixed size)
P quota (P limited, fixed size)

Figure S7.